J. Fluid Mech. (2001), *vol.* 432, *pp.* 1–30. Printed in the United Kingdom

Contact angles for evaporating liquids predicted and compared with existing experiments

By S. J. S. MORRIS

Department of Mechanical Engineering, University of California, Berkeley, CA 94720, USA
e-mail: morris@me.berkeley.edu

(Received 21 May 1999 and in revised form 30 September 2000)

The stationary meniscus of an evaporating, perfectly wetting system exhibits an apparent contact angle Θ which vanishes with the applied temperature difference ΔT, and is maintained for $\Delta T > 0$ by a small-scale flow driven by evaporation. Existing theory predicts Θ and the heat flow q_* from the contact region as the solution of a free-boundary problem. Though that theory admits the possibility that Θ and q_* are determined at the same scale, we show that, in practice, a separation of scales gives the theory an inner and outer structure; Θ is determined within an inner region contributing a negligible fraction of the total evaporation, but q_* is determined at larger scales by conduction across an outer liquid wedge subtending an angle Θ. The existence of a contact angle can thus be assumed for computing the heat flow; the problems for Θ and q_* decouple. We analyse the inner problem to derive a formula for Θ as a function of ΔT and material properties; the formula agrees closely with numerical solutions of the existing theory. Though microphysics must be included in the model of the inner region to resolve a singularity in the hydrodynamic equations, Θ is insensitive to microphysical detail because the singularity is weak. Our analysis shows that Θ is determined chiefly by the capillary number $Ca = \mu_\ell V_\ell/\sigma$ based on surface tension σ, liquid viscosity μ_ℓ and a velocity scale V_ℓ set by evaporation kinetics. To illustrate this result of our asymptotic analysis, we show that computed angles lie close to the curve $\Theta = 2.2Ca^{1/4}$; a small scatter of $\pm 15\%$ about that curve is the only hint that Θ depends on microphysics. To test our scaling relation, we use film profiles measured by Kim (1994) to determine experimental values of Θ and Ca; these are the first such values to be published for the evaporating meniscus. Agreement between theory and experiment is adequate; the difference is less than $\pm 40\%$ for 9 of 15 points, while the scatter within experimental values is $\pm 25\%$.

1. Introduction

Temperature control by evaporation of perfectly wetting liquids is fundamental to heat pipes and like devices. Since the static contact angle Θ_0 vanishes for perfectly wetting systems, part of the solid is covered with a non-evaporating uniform film. The measured thickness of that equilibrium film is usually a few nanometres (Kim 1994); it varies inversely with the applied temperature difference. Though the wall temperature exceeds the saturation temperature at which the phases coexist at common pressure, the solid attracts the liquid by van der Waals forces more strongly than the vapour, allowing the superheated liquid to coexist with its vapour across the interface of the equilibrium film. As the equilibrium thickness is less than the wavelength of light,

the visible film has an apparent contact line. Except in high-temperature heat pipes, the liquid is non-metallic, and poorly conducting relative to the solid. Consequently, heat flow is concentrated near the apparent contact line, and is determined by the structure of the contact region.

The apparent contact angle Θ is an essential part of that structure. Though Θ_0 vanishes for perfectly wetting systems, a non-zero contact angle is seen in experiments when the wall is heated to drive evaporation (Kim 1994, and references therein). That angle exists even if the interface is stationary relative to the wall, as in Kim's experiments and in heat pipes. The interface can be stationary if there is negligible resistance to liquid flow, except within the contact region itself. Evaporation of liquid increases the interfacial curvature locally, and so reduces the liquid pressure relative to that at infinity. Liquid thus flows from infinity towards the contact region, making a steady state possible. The pressure difference driving the liquid distorts the interface at film thickness ~ 10–$100\,\mathrm{nm}$, and so creates the contact angle; unlike Θ_0, the apparent contact angle Θ is thus a flow property.

To establish the significance of Θ, I have shown elsewhere that there is a separation of scales in practice; Θ is established within a small-scale inner region contributing a negligible fraction of the evaporation, while heat flow occurs in a large-scale outer geometry specified by Θ (Morris 2000). The heat flow can thus be found by solving Laplace's equation for the temperature subject at the interface to Newton's law of cooling with a predicted heat transfer coefficient. That conduction model is derived initially by scaling and self-consistency arguments, but is then verified by comparing its predictions with those of detailed simulations by Stephan & Busse (1992). My analysis of the heat flow differs from others assuming a contact angle, as I derive and test conditions sufficient for the conduction model to describe a particular system. The analysis does not determine Θ, because it is based on requiring self-consistency of a simplified model of heat flow, rather than on analysis of a complete model of the contact region as a free-boundary problem.

Here, we supplement the conduction model by deriving and testing against Kim's experiments a formula for the apparent contact angle of a stationary meniscus. To predict Θ, we analyse a version of a free-boundary problem posed by Potash & Wayner (1972), in which creeping flow is coupled to conduction, kinetics, thermodynamics and interfacial conditions. Fluid motion and heat flow are coupled since pressure differences within the liquid affect the evaporation kinetics directly; they also shape the film and so affect the heat flux. Microphysics enters through the disjoining pressure Π, i.e. the resultant van der Waals force exerted on a unit interfacial area by the solid, liquid and gas. The disjoining pressure is essential to the model as it prevents a velocity singularity by setting a minimum scale. Moosman & Homsy (1980) saw that as Θ^2 is usually small, lubrication theory can be used to reduce the model to a pair of ordinary differential equations for the film thickness and liquid pressure. DasGupta *et al.* (1993) state the version of the theory used by Kim & Wayner (1996) to interpret Kim's experiments. In that version, the liquid and gas are chemically identical, but in the experiments, the gas is a mixture of vapour and inert components (air). Kim & Wayner tacitly assume that the existing theory can be applied if the thermodynamic properties of the mixture are taken as those of the pure vapour at the wall temperature and corresponding coexistence pressure.

To clarify the formulation, in § 2 we extend the existing theory to include a gas consisting of vapour and an inert component. We show explicitly how the partial pressure of vapour is determined. We also show that for the important case in which the interface curvature vanishes far from the wall, our dimensionless boundary-value

problem (7) can be made identical with that for a chemically pure system by an appropriate choice of scales. To outline our logic, we need the definition of the Biot number β based on equilibrium film thickness H_s, liquid conductivity K_ℓ, and the heat transfer coefficient h defined by (4*f*); it is $\beta = hH_s/K_\ell$, i.e. the ratio of H_s to the adjustment thickness $L = K_\ell/h$ on which the interface temperature varies from its value in the equilibrium film to its value at infinity (Morris 2000, p. 60). Commonly, $\beta \ll 1$.

In § 3, we give an operational definition (8) for the apparent contact angle, i.e. a definition allowing Θ to be extracted unambiguously from measured film profiles. The definition is non-trivial as it involves understanding the various scales at which curvature is important; it is essential to our comparison of theory and experiment. Our definition is new; though the existing theory is used in the heat transfer literature to compute contact angles, ours is the first comparison of measured and predicted values. We then establish the significance of our definition (8) by showing that the angle we define appears naturally in the formula (10) for the heat flow q_*, i.e. the spatially integrated flux, across the entire contact region.

In § 4, we use numerical solutions of problem (7) to show the development of the inner and outer structure as $\beta \to 0$; the conduction resistance H_s/K_ℓ to heat flow across the film is then small compared with the interfacial resistance h^{-1} to evaporation. In § 5, we analyse the inner region defined by $\beta \to 0$ with the film thickness of order H_s. Within this region, the conduction resistance is negligible and the film is isothermal. The inner region does not define the contact angle by itself, for although H_{xx} vanishes at its outer edge, the slope there varies slowly with x according to the formula $H_x \propto \sqrt[4]{\ln(x/k)}$. Analysis of an outer region is needed to predict Θ; microphysics affects that region only through the integration constant k.

To interpret k, we then show that the same behaviour for H_x occurs in a purely hydrodynamic model of the inner region containing no thin film effects; neither the disjoining pressure, nor the effect of pressure on kinetics is included. As the disjoining force is essential to setting the minimum scale in (7), its absence from the simplified model requires us to impose a scale; we take the domain as semi-infinite, and give a film thickness a at the origin. Because k is now determined by the parameter a, we infer that in (7), the overall effect of microphysics is to set a scale for the outer solution; that solution depends weakly on a because the singularity in the hydrodynamic model for $a \to 0$ is weak.

In § 6, we complete the prediction of Θ by analysing the outer region, in which the interface temperature falls from its uniform value within the inner region to its value at infinity. For this to occur, the film must be thick enough for its conduction resistance to be significant, although that of the thin inner film is negligible. The outer limit is thus defined by $\beta \to 0$ with film thickness of order the adjustment scale. In this region, thin-film effects are negligible, as at the outer edge of the inner region. Since H_x varies slowly with x at the outer edge of the inner region, we find the outer thickness to vary linearly with x at leading order; so Θ is determined by the inner region, while heat flow is confined to the outer region. This picture is consistent with that in Morris (2000).

In § 7, we combine results from §§ 5 and 6 to obtain a formula for Θ. We predict analytically that Θ depends only on the capillary number Ca based on the velocity scale set by evaporation, and the Biot number B based on the lengthscale k set by microphysics; we confirm this prediction numerically. Our formula shows that Θ depends weakly on the microphysical parameter B. To illustrate this result, we show that computed values of Θ satisfy the relation $\Theta/Ca^{1/4} = 2.20 \pm 0.25$ for the range of

B occurring in practice; the dependence of Θ on microphysics is thus manifested as a small scatter about a curve in the (Θ, Ca)-plane. To interpret this result, in § 8 we extend our hydrodynamic model of the inner region to include the outer region. We infer that if the Biot number based on the microphysical scale is small, the prediction for Θ depends only weakly on the specific microphysical model used. To illustrate this, we show that Hocking's (1995) analysis of the evaporating meniscus of a partially wetting liquid yields a like formula for Θ.

In § 9, we determine the heat flow q_*. In § 10, we verify our prediction for Θ against experimental values we infer from film profiles measured by Kim (1994). Our use of the experiments differs essentially from that of Kim & Wayner (1996). They fit the entire computed profile to an observed profile by adjusting the dispersion constant A appearing in the equation for the disjoining force; so they use a non-equilibrium process to measure the equilibrium property A. Though they use the fitted profile to evaluate the local slope at two different film thicknesses, they neither predict nor measure the apparent contact angle as defined here. By contrast, we stress the definition, prediction and inference of contact angles because Θ is a portable quantity; a value inferred from one flow can used to predict heat flow in another.

In § 10, we also give a new method for measuring the applied temperature difference ΔT. As ΔT is too small to measure with a thermocouple, Kim infers it from the equilibrium film thickness H_e measured by ellipsometry. However, as the relation (29) between ΔT and H_e depends linearly on the dispersion constant A, his method introduces a much stronger dependence on microphysics than that existing in the physical problem. That difficulty does not arise in our method. We show that since $\beta \ll 1$ in the experiments, ΔT can be inferred from q_* by solving a conduction problem in which we account for interface curvature. The result is equation (30) giving ΔT in terms of known material properties and measurable quantities: namely Θ, the radius of curvature R of the large-scale interface, and the total heat flow q_* inferred from the evaporation rate. For just one experiment, Kim measured the total evaporation rate; for that case, values given by the two methods agree closely. Our method involves neither microphysics, nor ellipsometry, for to infer Θ, we use only the part of the film profile measured by interferometry.

In § 11, we relate this study to my previous work, in which scaling is used to derive conditions sufficient for q_* to be determined by a conduction problem. We show here that those conditions (Morris 2000, equations (3*a*)–(3*c*)) are satisfied if $\beta \to 0$; as claimed there, this analysis implies the conduction model.

To end this introduction, we explain how the prediction of contact angles for the stationary evaporating meniscus differs from the prediction of the dynamic contact angle for a spreading isothermal drop; these problems are limiting cases for a spreading volatile drop. The contact angle for the stationary evaporating meniscus is a property of the small-scale flow driven by evaporation; it is independent of the large-scale geometry if the pressure difference across the large-scale interface is vanishingly small compared with that across the interface of the equilibrium film. Specifically, our equation (10*b*) implies that in the limit of vanishing large-scale curvature, the slope approaches a limit far from the apparent contact line.

For isothermal spreading, the situation is slightly more complicated. Following Tanner (1979), a quasi-steady problem for the film thickness can still be posed by taking axes moving with the contact line, and imposing a constant curvature at infinity. However, in the limit of vanishing large-scale curvature, the slope here does not approach a limit as $x \to \infty$ but instead continues to vary weakly as $(\ln x)^{1/3}$ (e.g. Joanny 1986, equation 38). Because the double limit does not exist, the contact angle

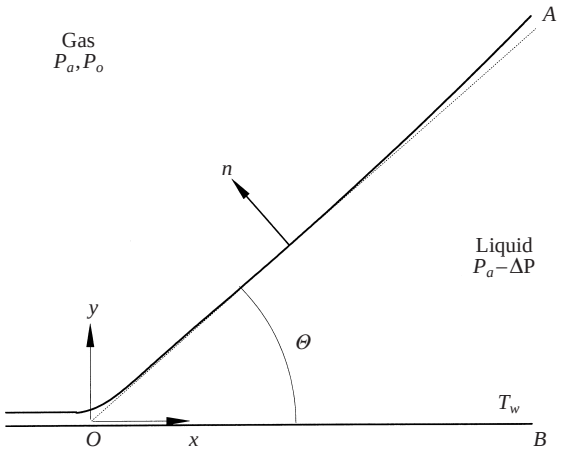

FIGURE 1. Definition sketch.

depends on the curvature of the large-scale meniscus; since the slope diverges only weakly with x, the curvature-dependence is weak, as can be seen from equation (7.22) of Cox (1986). The spreading problem differs from that of the stationary meniscus owing to a weak, but essential, dependence on the large-scale curvature.

Even in the spreading problem, the outer geometry influences the contact angle only through a length scale. So in either problem, Θ can be determined from a local analysis, and it is not necessary to follow Hocking (1995) in incorporating details of the outer geometry in the formulation. We thus abstract the idea of a contact angle from the detail of the large-scale geometry, so that Θ becomes a portable quantity like the static contact angle Θ_0.

2. Boundary-value problem

We start with terminology and notation. Figure 1 shows the geometry. We extend the existing theory of the evaporating meniscus by assuming that the liquid is chemically pure, but that the atmosphere consists of two components: one is inert; the other is the vapour phase of the liquid. This formulation includes as a special case that of DasGupta *et al.* in which the gas is pure vapour. As shown in figure 1, the total gas pressure is P_a, and the local value of the partial pressure of vapour is P_v; at infinity, P_v approaches the uniform value P_o. The saturation temperature T_o is defined as the temperature at which the liquid and its vapour phase coexist when both are at common pressure P_o. The uniform temperature at infinity is T_∞, and the uniform wall temperature is $T_w \geqslant T_\infty$. (Analysis of the meniscus on a conducting slab shows that for small liquid–solid conductivity ratios K_ℓ/K_s, it is a good approximation to assume uniform wall temperature for computing Θ. Figure 8 of Morris (2000) shows that for $K_\ell/K_s \to 0$, the solid temperature varies only at a scale large compared with the adjustment thickness L. Because Θ is established at a scale smaller than L, it can be calculated by taking T_w as uniform.) Subscripts ℓ and v denote the liquid and its vapour phase. All properties are evaluated at the wall temperature. The sound speed of the vapour phase is C, and the specific heat ratio is γ. The thermal conductivity, latent heat, dynamic viscosity, density and surface tension are K, Q, μ, ρ and σ.

Next, we give the simplifying assumptions; they are the same as those of DasGupta *et al.* We take the interface as stationary relative to the wall, and the interface slope

as small. We assume $(T_w - T_\infty)/T_\infty \ll 1$; so we take the temperature as uniform to calculate material properties. We take convective nonlinearities as negligible since the Reynolds and Péclet numbers based on the total evaporation rate are small. Lastly, we discuss the equation for Π. Miller & Ruckenstein (1974) show that if the interface slope is small, the disjoining pressure Π at a point is determined by the local film thickness H. We assume that $\Pi = A/H^3$, where A is the dispersion constant. Though Levinson *et al.* (1993, figure 3) show experimentally that this relation holds only at thicknesses less than a few nanometres, we use it for all H as a model to prove that Θ and q_* are insensitive to microphysics for perfectly wetting liquids.

Now we describe the kinetic equation. Let $\mathscr{P}(P_\ell, T)$ be the coexistence pressure; i.e. the partial pressure of vapour required for the liquid to coexist with its vapour phase at temperature T when the liquid pressure is P_ℓ. Also, let $\lambda = \sqrt{2\gamma/\pi}$. By kinetic theory, the evaporative mass flux J at a point on the interface is related to the local values of the temperature T, liquid pressure P_ℓ and partial pressure P_v by the equation $CJ/\lambda = \mathscr{P}(P_\ell, T) - P_v$; see Cammenga (1980, equations 29 and 65). So liquid evaporates if the local partial pressure of its vapour phase is less than the local coexistence pressure $\mathscr{P}$. Small pressure differences exist within the gas to push vapour created at the interface to infinity. Like DasGupta *et al.*, we assume these pressure differences to be negligible compared with P_o, so that $P_v = P_o$; we thus assume that the evaporation rate is determined by processes within the liquid. By the assumption $P_v = P_o$, and the definition of $\mathscr{P}$, $\mathscr{P}(P_o, T_o) = P_o$. So the kinetic equation can be written $CJ/\lambda = \mathscr{P}(P_\ell, T) - \mathscr{P}(P_o, T_o)$. As departures from thermodynamic equilibrium are small in practice, we linearize the right-hand side of this expression.

Next, we give the dimensional governing equations. In the limit of vanishing interface slope, the film thickness $H(x)$, interface temperature $T(x)$, evaporative mass flux $J(x)$ and liquid pressure $P_\ell(x)$ satisfy

$$\left.\begin{aligned} \rho_\ell \frac{\mathrm{d}}{\mathrm{d}x}\left(H^3 \frac{\mathrm{d}P_\ell}{\mathrm{d}x}\right) &= 3\mu_\ell J, \\ \rho_\ell CJ/(\lambda\rho_v) &= (P_\ell - P_o) + \rho_\ell Q(T - T_o)/T_o \\ K_\ell(T_w - T)/H = QJ, \quad P_a - P_\ell &= \sigma \frac{\mathrm{d}^2 H}{\mathrm{d}x^2} + A/H^3 \end{aligned}\right\} \quad \text{for} \quad -\infty < x < \infty, \quad (1a\text{–}d)$$

$$P_\ell \to P_{\ell\infty}, \quad T \to T_\infty \quad \text{as} \quad x \to \infty, \qquad (1e, f)$$

$$\frac{\mathrm{d}H}{\mathrm{d}x} \to 0 \quad \text{as} \quad x \to -\infty. \qquad (1g)$$

In (1f), $P_{\ell\infty} = P_a - \Delta P$. Similar equations are posed by Moosman & Homsy (1980), and DasGupta *et al.* (1993); however, (1) differs slightly from those formulations, as we discuss in the next two paragraphs.

We now interpret problem (1). (i) In writing the mass balance (1a), we assume no slip at the wall, and no shear stress at the interface. We thus take the thermocapillary stress as negligible; we justify this assumption in Appendix A. (ii) The linearized kinetic equation (1b) involves the partial pressure P_o, not the total pressure P_a. (iii) The enthalpy balance (1c) states that all heat conducted from the wall is absorbed as latent heat at the interface; this equation is a consistent approximation to the exact jump condition given by Delhaye (1974, equation 27). (iv) The normal stress balance (1d) is affected by the inert gas since the resultant pressure force $P_a - P_\ell$ on

an interfacial element depends on the total gas pressure P_a, not merely on the partial pressure P_o. Equation (1*d*) differs from the corresponding equation (1) in DasGupta *et al.* (1993); there the gas is taken as pure vapour. (v) We shall see following (2) that for the problem to be well posed either P_o or T_∞ must be given, as in boundary condition (1*f*). (vi) Boundary condition (1*g*) ensures that no horizontal mass flow is imposed on the film at $-\infty$.

The kinetic equation (1*b*) differs in one essential from the corresponding equation (4) of DasGupta *et al.* (1993). There, instead of the saturation temperature T_o and partial pressure P_o, we see the temperature T_∞ and what they call 'the bulk vapor pressure of the liquid at temperature' T_∞, i.e. $\mathscr{P}(P_o, T_\infty)$. By their (19), we see that $P_\ell \not\to \mathscr{P}(P_o, T_\infty)$ at infinity. The evaporation rate predicted by their kinetic equation (4) therefore does not vanish at infinity. However, the heat flux to the interface vanishes as $H \to \infty$ by our (1*c*) (their equation 6). So their formulation does not conserve energy exactly; our formulation does, since the condition $J \to 0$ at infinity determines the partial pressure P_o, as we now show.

By using the condition that $J \to 0$ at infinity in the kinetic equation (1*b*), we obtain

$$0 = (P_{\ell\infty} - P_o) + \rho_\ell Q(T_\infty - T_o)/T_o, \quad \text{so } (T_\infty - T_o)/T_o = -(P_{\ell\infty} - P_o)/(\rho_\ell Q). \quad (2a,b)$$

Equation (2*b*) gives T_o and $P_o = \mathscr{P}(P_o, T_o)$ as functions of the boundary values $P_{\ell\infty}$ and T_∞; so either T_∞ or P_o must be given for the problem to be well-posed. This equation formulates the Kelvin effect; when the pressure $P_{\ell\infty}$ in the liquid is less than that P_o in the vapour, molecules tend to stick to the interface, allowing the phases to coexist at a temperature T_∞ higher than that T_o at which they coexist at common pressure P_o; see Fisher & Israelachvili (1981) for experimental confirmation.

We can now eliminate P_o and T_o from (1). By subtracting (2*a*) from (1*b*),

$$\rho_\ell CJ/(\lambda\rho_v) = P_\ell - P_{\ell\infty} + \rho_\ell Q(T - T_\infty)/T_o. \quad (3)$$

In the last term, T_o can be replaced by T_∞ as $|T_\infty - T_o|/T_o \ll 1$ in practice. So P_o and T_o are eliminated, and the formulation conserves energy. Our problem now consists of (1) with (1*b*) replaced by (3).

Next, we define scales. Let $\Delta T = T_w - T_\infty$, and $\mathrm{T} = \Delta T/T_o$. Also let

$$P_s = \rho_\ell Q\mathrm{T}, \quad H_s = (A/P_s)^{1/3}, \quad L_s = (\sigma H_s/P_s)^{1/2}, \quad \Theta_s = H_s/L_s, \quad (4a\text{–}d)$$

$$V_\ell = \lambda\rho_v Q\mathrm{T}/(\rho_\ell C), \quad h = \rho_\ell Q V_\ell/\Delta T = \lambda\rho_v Q^2/(CT_o). \quad (4e,f)$$

In (4*a*), $\lambda = \sqrt{2\gamma/\pi}$, as defined in the paragraph preceding (1). We show, following (6), that P_s is the pressure difference $P_{\ell\infty} - P_\ell(-\infty)$ within the liquid. Next, the definitions of H_s and L_s ensure that all three terms in the normal stress balance (1*d*) are comparable when the pressure difference across the interface is of order P_s; Θ_s is the corresponding unit of slope. Both lengthscales are typically nanometres; in the example of Stephan & Busse (1992), $H_s = 0.9\,\mathrm{nm}$, and $L_s = 3\,\mathrm{nm}$. Further, the velocity scale V_ℓ for the liquid flow normal to the interface is obtained from the kinetic equation (3) by writing $J \sim \rho_\ell V_\ell$, and balancing terms. Moreover, h is the evaporative heat transfer coefficient, as in Cammenga (1980, p. 405); the pressure term in (3) is negligible if $|P_\ell - P_{\ell\infty}| \ll P_s$, which holds in thick films for which $H \gg H_s$. Equation (3) then reduces to $J = \lambda\rho_v Q(T - T_\infty)/(CT_o)$, and the heat flux $QJ = h(T - T_\infty)$, where h is given by (4*f*). Lastly, for use below, we note the existence of a second pressure scale; from the continuity equation, the tangential velocity scale $U_\ell = L_s V_\ell/H_s$, and from U_ℓ and the lubrication equation we find that a pressure difference of order $P_f = 3\mu_\ell L_s^2 V_\ell/H_s^3$ is needed to drive flow at the scale H_s.

$\epsilon = \Delta P/P_s$	$\beta = hH_s/K_\ell$	$f = 3\mu_\ell L_s^2 V_\ell/(P_s H_s^3)$	$Ca = \mu_\ell V_\ell/\sigma$
0.000009	0.2	0.2	0.0009
0.004	0.02	1.3	0.002
0.06	0.01	7	6×10^{-9}

TABLE 1. Parameters in the theory. Scales are defined by (4).

In the rest of this work, dimensional variables are starred. A subscript x denotes differentiation. We define the dimensionless liquid pressure P, interface temperature T, film thickness H, position x and evaporative mass flux J by

$$P = (P_{*\ell} - P_{\ell\infty})/P_s, \quad T = (T_* - T_\infty)/\Delta T, \quad H = H_*/H_s,$$
$$x = x_*/L_s, \quad J = J_*/(\rho_\ell V_\ell). \tag{5a–e}$$

We non-dimensionalize using $\Delta T = T_w - T_\infty$ rather than the superheat $T_w - T_o$. Though our dimensionless problem (7) thus differs from that of DasGupta *et al.*, ΔT has a physical significance which $T_w - T_o$ lacks; the heat flow varies with ΔT, but T_o does not occur within the flow unless the interface is linear at infinity.

The dimensionless form of (1) is

$$(1 - T)/H = \beta J, \quad J = P + T, \quad (H^3 P_x)_x = fJ, \quad \epsilon - P = H_{xx} + 1/H^3, \tag{6a–d}$$

$$H_x \to 0, \quad \text{as} \quad x \to -\infty, \qquad P \to 0, \quad \text{as} \quad x \to \infty. \tag{6e,f}$$

The dimensional pressure difference within the liquid is P_s since (6) implies that $P \to -1$ as $x \to -\infty$.

Problem (6) contains three independent parameters, namely ϵ, f and β. The pressure ratio $\epsilon = \Delta P/P_s$ compares the pressure difference ΔP across the interface at infinity to the pressure difference P_s driving the liquid flow. ϵ determines if there is motion or not. The motion is negligible in the limit $T_w - T_\infty \to 0$; then $P_s \to 0$, and $\epsilon \to \infty$. Because $|P| \leqslant 1$, the left-hand side of (6*d*) can then be approximated by ϵ so that the interface shape is not affected by the motion. At the other extreme, $P_s \gg \Delta P$ so that $\epsilon \to 0$. The interface is then strongly perturbed by the flow; we shall see that a well-defined apparent contact angle then exists. The other parameters f and β control the structure of the resulting flow. The flow resistance $f = P_f/P_s$ measures the viscous resistance to evaporation. Lastly, as previously defined, the Biot number $\beta = hH_s/K_\ell$ determines the ratio of the conduction resistance of the liquid film to the interfacial resistance.

In table 1, we give the definitions of ϵ, β and f in terms of the scales defined by (4); we also give typical values for these parameters and for the capillary number $Ca = \mu_\ell V_\ell/\sigma$. Numerical values in rows one and two are for the simulations of Stephan & Busse (1992), and Schonberg, Das Gupta & Wayner (1995, case 2 of table 1). Those in the third row are for the experiments of Kim (1994, case 4 of table 5.1); they typify the values given for his experiments in our table 2. Table 1 shows that usually $\epsilon \ll \beta \ll 1$, and $f \sim 1$. The exception is that in Kim's experiments ϵ is not small; we discuss the significance of this following figure 2.

Like Moosman & Homsy (1980), we express (6) in terms of P and H alone by eliminating T between (6*a*) and (6*b*). So $J = (1 + P)/(1 + \beta H)$. By substituting for J

in (6*c*), we obtain

$$(H^3P_x)_x = f(1+P)/(1+\beta H), \quad \epsilon - P = H_{xx} + 1/H^3 \quad \text{for} \quad -\infty < x < \infty, \tag{7a,b}$$

$$H_x \to 0 \quad \text{as} \quad x \to -\infty, \qquad P \to 0, \quad \text{as} \quad x \to \infty. \tag{7c,d}$$

Problem (7) is solved by standard shooting methods, as in DasGupta *et al.* (1993).

For $\epsilon \neq 0$, (7) differs from the corresponding problem of DasGupta *et al.* (1993, equations 15–19) owing to a different choice of scales. For arbitrary ϵ, our problem can be transformed into that of DasGupta *et al.* by a linear transformation in which the coefficients depend on ϵ.

3. Definition and significance of Θ

Though the theory of the evaporating meniscus is often used to compute contact angles, a precise definition of Θ has not been given before. Such a definition is essential to our comparison of theory with experiment. By (7*b*,*d*), $H_{xx} \to \epsilon$ as $H \to \infty$, and it can be verified that for $\epsilon \neq 0$, problem (7) admits a solution such that $H \sim \frac{1}{2}\epsilon x^2 + c_0 x + c_1$; here, c_0 and c_1 are integration constants. If the parabola so defined has a zero, a contact angle is defined by the slope at $H = 0$. An apparent contact angle is thus defined by first computing (or observing) the constant curvature profile for large H, and then extrapolating it to $H = 0$. Of course, the apparent contact line and contact angle so defined will coincide with what is observed optically only if the entire observed interface has constant curvature. Because we shall see that in the experiments, the curvature becomes uniform only at film thicknesses exceeding the smallest measured thickness, we need a way to identify the region of uniform curvature in measured profiles; two-fold differentiation of data is not practicable as each differentiation amplifies noise.

To identify the constant-curvature region, we multiply the asymptotic relation $H_{xx} \sim \epsilon$ by $2H_x$, and integrate in x to show that $H_x^2 \sim 2\epsilon H + \tilde{b}^2$, where $\tilde{b}$ is an integration constant. When the interface curvature is constant, a plot of H_x^2 against H is therefore linear; the curvature and squared contact angle are found from the slope and intercept of that line. As the solution of (7) depends on the parameters β, ϵ and f, so does the integration constant $\tilde{b}$. From table 1, we see that of the three parameters, only ϵ depends on the large-scale geometry (through ΔP). For $\epsilon \to 0$, the apparent contact angle is therefore a property of the small-scale flow alone; otherwise it depends on ϵ, and so on the large-scale geometry. The importance of the limit in defining the contact angle for evaporating systems has not been previously recognized.

We therefore define the apparent contact angle by $\Theta = \Theta_s b$, where

$$b^2 = \lim_{\epsilon \to 0} \lim_{H \to \infty} (H_x^2 - 2\epsilon H) \quad \text{so that} \quad \Theta/(3\,Ca)^{1/4} = b/f^{1/4}. \tag{8a,b}$$

Here, we have used the identity $\Theta_s = (3\,Ca/f)^{1/4}$, which follows from the definitions of P_f, L_s, Θ_s and Ca. In the definition (8*a*), the inner limit $H \to \infty$ picks out the constant curvature part of the interface; by the previous paragraph, the argument of the limit then approaches the constant $\tilde{b}^2$. This inner limit also ensures that the apparent contact angle defined by (8) is independent of film thickness. The outer limit $\epsilon \to 0$ ensures that the apparent contact is determined purely by the small-scale flow. By (8*a*), $b(\beta, f) = \lim_{\epsilon \to 0} \tilde{b}$; we call b the slope parameter, and $\tilde{b}$ the false slope parameter. The precise definition (8) is essential as the term 'apparent contact angle' is used loosely in the literature, as we discuss in § 10.

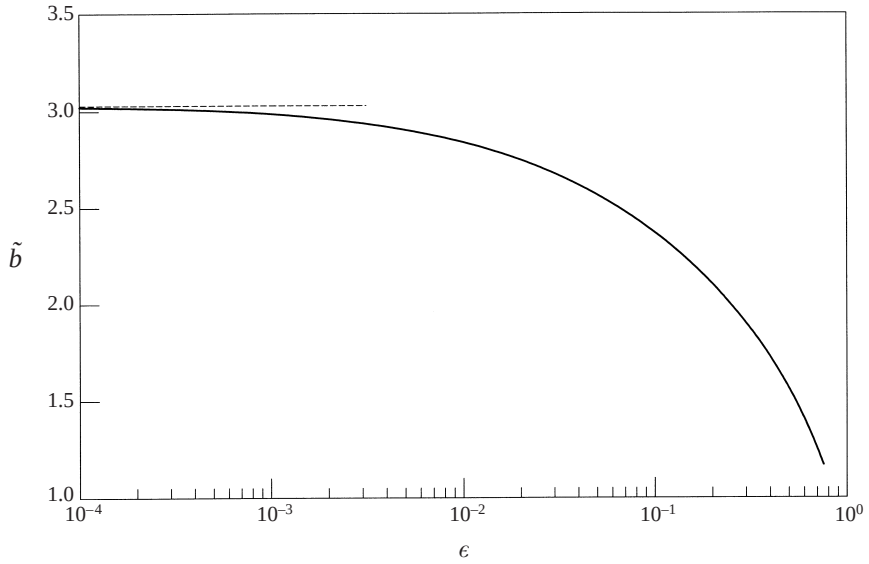

FIGURE 2. False slope parameter $\tilde{b}$ computed for $\beta = 0.01$ and $f = 7$ as a function of ϵ without approximation from the solution of problem (7). As defined below (8), $\tilde{b}^2 = \lim_{H\to\infty}(H_x^2 - 2\epsilon H)$. The parameters β and f are defined in table 1.

Figure 2 illustrates the approach to the limit (8*a*) by showing the false slope parameter $\tilde{b}$ as a function of ϵ for $\beta = 0.01$ and $f = 7$; these values are for Kim's experiment summarized in row 3 of table 2. For the value $\epsilon = 0.06$ appropriate to Kim's experiment, the figure shows that $\tilde{b} \doteqdot 2.5$, while the limiting value $b = 3.03$. So the experimental value of the contact angle inferred from that measured profile is likely to be $\sim 20\%$ too low owing to the effect of large-scale curvature; as we shall see at the end of § 10, the discrepancy is even larger for some experiments. This example shows that in the experiments, the contact angle depends to some degree on the pressure difference applied across the large-scale interface. By contrast, we see from table 1, that in typical applications ϵ is small enough for Θ to be a flow property. (ϵ is smaller in applications than in Kim's experiments because the applied temperature difference is larger in applications.)

Next, we demonstrate the significance of Θ for the heat flow. The dimensional heat flux at x is $(K_\ell \Delta T/H_e)(1-T)/H$, i.e. $(K_\ell \Delta T/H_e)(\beta/f)(H^3 P_x)_x$, by (6*a*) and (6*c*). The rate $q_*(x)$ at which heat flows across the interval $(-\infty, x)$ of the film is found by integration in x. So

$$\Theta q_*/(K_\ell \Delta T) = (\beta b/f) H^3 P_x. \tag{9}$$

Here, (8) has been used to replace bH_s/L_s by Θ. The total heat flow $q_*(x)$ between $-\infty$ and x is proportional to the mass flow rate $H^3 P_x$ at x because all mass flowing past point x towards $-\infty$ is evaporated between $-\infty$ and x. In the rest of this paper we study the case $\epsilon = 0$; we treat the effect of a small non-zero curvature on the outer meniscus in a subsequent paper.

We can now find the heat flow for large x. For $\epsilon = 0$, (7) admits a solution in which $H \sim bx$ as $x \to \infty$. (Equation (8*a*) is then satisfied trivially.) For large x, the solution thus exhibits an apparent contact line; we take $x = 0$ there. For $x \to \infty$, the

right-hand side of (7*a*) simplifies since $P \sim 0$ and $H \sim bx$. By integration,

$$H^3 P_x = \frac{f}{\beta b} \ln\left(\frac{x}{\delta}\right) + o(1), \quad H_x = b - \frac{f}{2\beta b^4} x^{-1} \ln x + o(1) \quad \text{as } \frac{x}{\delta} \to \infty. \qquad (10a, b)$$

Here, δ is an integration constant. We give the second term in (10*b*) to stress that H_x approaches a limit at infinity. As stated in § 1, unlike the meniscus of a spreading drop, the stationary evaporating meniscus has a well-defined contact angle that is a property solely of the small-scale flow.

The heat flow is given for large x by (10*a*) and (9) as

$$q_* \Theta / (K_\ell \, \Delta T) = \ln(x/\delta) + o(1). \qquad (11)$$

To interpret this result, we recall that the interface temperature $T \to 0$ at infinity, by (1*a*). Far from the apparent contact line, problem (7) thus describes conduction in a wedge of angle Θ bounded by the isotherms $T = 1$ (wall) and $T = 0$ (interface). The heat flux across the wedge varies asymptotically as $1/x$, so that the heat flow varies as $\ln x$, as in (11).

The contact angle Θ defined by (8) thus appears naturally in the outer limit (11) of the heat flow. Next, we predict Θ for the case $\beta \to 0$ usual in applications. As part of the analysis, we deduce the conduction model for heat flow in the contact region.

4. Effect of vanishing Biot number

To begin, we use numerical solutions to illustrate the development of the solution as $\beta \to 0$. Figure 3 shows the interface temperature T and evaporative mass flux J as a function of $x = x_*/L_s$, where L_s is defined by (4*c*). The curves are computed without approximation from (7) for $\epsilon = 0$. We see that as $\beta \to 0$ with H fixed, $T \to 1$; the interface temperature approaches the wall temperature as the conduction resistance vanishes. Though the inner film is nearly isothermal, the curve for J shows there is still evaporation from it; by (6*a*, *b*) with $\beta = 0$, $J = 1 + P$ which is not zero as neither H nor P is uniform. The pressure difference driving this flow distorts the interface and creates the contact angle. The figure also shows that the isothermal region asymptotically contributes a negligible fraction of the evaporation because the region to the left of the plateau in J contributes an amount of order unity to the integral of J, while the contribution of the plateau increases with plateau length. Figure 3 suggests the existence for small β of a separation of scales such that Θ is established at small scales, while evaporation occurs across the large-scale outer meniscus. Next, we quantify this structure by asymptotic analysis.

5. The inner isothermal region

We define the inner limit, as in § 1, by $\beta \to 0$ with fixed H and f. In that limit, (7) simplifies to

$$(H^3 P_x)_x = f(1 + P), \quad -P = H_{xx} + 1/H^3 \quad \text{for} \quad -\infty < x < \infty, \qquad (12a, b)$$

$$P = -1 \quad \text{as} \quad x \to -\infty, \qquad P \to 0 \quad \text{as} \quad x \to \infty. \qquad (12c, d)$$

Boundary condition (7*d*) on P at infinity is applied here to the inner solution as we prove, following (15), that the pressure difference in the outer region is negligibly small in β.

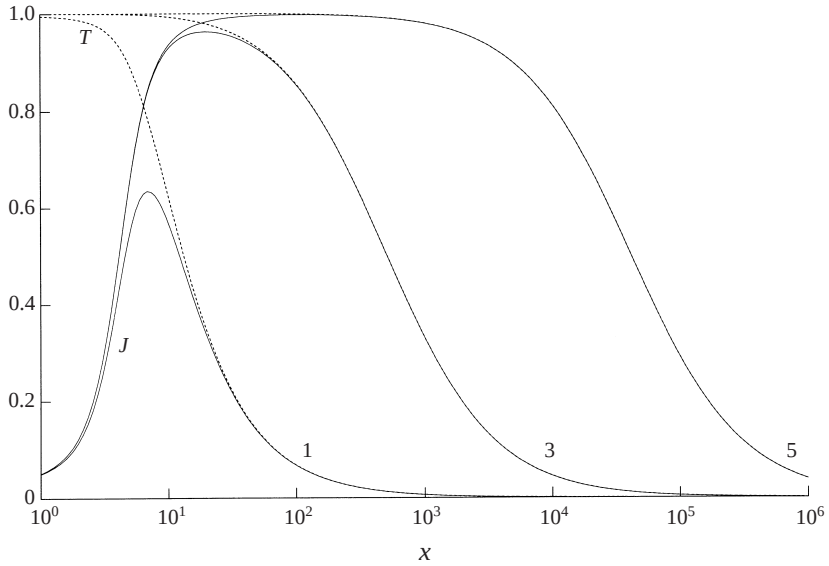

FIGURE 3. Numerical solution of problem (7) for $f = 1$ and the values of $-\log_{10}\beta = 1, 3$ and 5 shown on the figure.

Problems (12) and (7) differ as the evaporation term on the right-hand side of (12a) does not vanish at infinity. Since the flow continues to distort the interface, we find that the slope does not approach a limit. To prove this we need the large x behaviour of the solution; that behaviour is also useful as it shows how microphysics affects Θ. From a numerical solution of (12), we find that H grows at infinity so as to make $1 \gg H_{xx} \gg 1/H^3$. The disjoining force $1/H^3$ is thus asymptotically negligible in (12b), so that $P \sim -H_{xx}$. Also, since $P \to 0$ by boundary condition (12d), the pressure term on the right-hand of (12a) is asymptotically negligible. Thin-film effects are thus negligible at the outer edge of the isothermal region, and the behaviour of (12) is asymptotically determined by the conditions $-P \sim H_{xx}$, $(H^3P_x)_x \sim f$ and $P(\infty) = 0$.

To interpret these conditions, we define a simplified hydrodynamic model by the problem

$$(\hat{H}^3\hat{P}_x)_x = 1, \quad \hat{P} = -\hat{H}_{xx} \quad \text{for} \quad 0 \leqslant x < \infty, \tag{13a,b}$$

$$\hat{H} = a, \quad \hat{H}_x = 0 = \hat{P}_x, \quad \text{at} \quad x = 0, \tag{13c,d,e}$$

$$\hat{P} \to 0, \quad \text{as} \quad x \to \infty. \tag{13f}$$

By comparing (13a,b) with the relations preceding them, we see that $P \sim f^{1/4}\hat{P}$ and $H \sim f^{1/4}\hat{H}$. Because this hydrodynamic model does not include the disjoining force, there can be no equilibrium film, and there is nothing to impose a minimum scale. To prevent a velocity singularity, we must impose a scale; so we take the domain as semi-infinite, and the initial thickness a as non-zero in (13c). Also, because the differential equations (13a,b) are invariant under the substitution $x \to -x$, they admit a solution in which $\hat{P}$ and $\hat{H}$ are even functions. By imposing the homogeneous boundary conditions (13d–f), we select that solution to ensure that Θ is determined as part of the solution, rather than being imposed upon it.

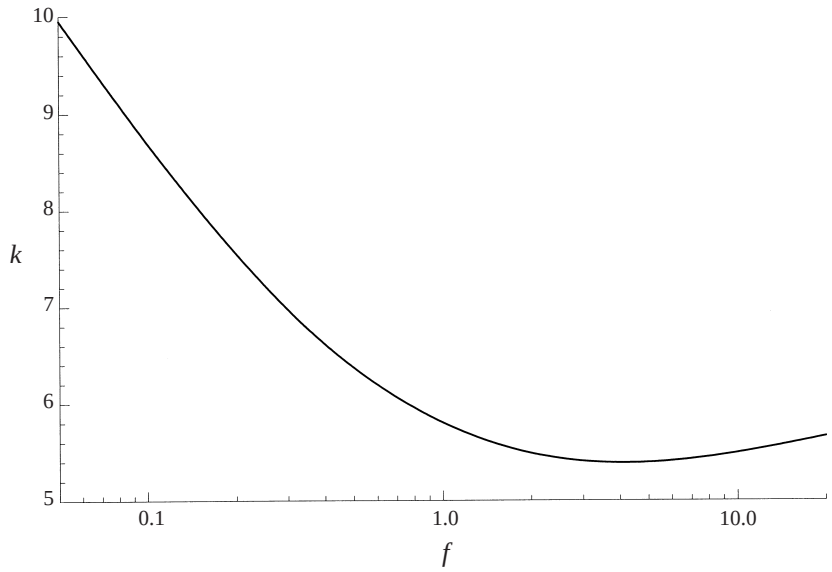

FIGURE 4. Scale k defined by (14) as a function of the flow resistance f defined in table 1.

We next discuss the large x behaviour of the solution of (13). We show in Appendix B that

$$\hat{H} \sim x(4z)^{1/4} \sum_{n=0}^{\infty} A_n z^{-2n} \quad \text{where} \quad z = \ln(x/k), \tag{14a,b}$$

k is an integration constant, and the first four coefficients are $A_0 = 1$, $A_1 = -21/64$, $A_2 = -16611/8192$ and $A_3 = -1099\,77903/26\,21440$. Because the series (14) is derived from (13), which is in effect an approximation to (12), we note that the error made by truncating (14) at any order is large compared with that made in deriving (13) from (12). (The truncation error is only logarithmically small in x; but the error made by approximating (12) by (13) is much smaller as the inequalities $1 \gg H_{xx} \gg 1/H^3$ hold with algebraically small error in x.) So all terms in (14) are significant for both problems (12) and (13).

The asymptotic series (14) describes a family of solutions parameterized by the integration constant k. The series satisfies the differential equations (13a, b) and the boundary condition (13f) at infinity. From this asymptotic series, we see that microphysics influences the outer solution only through the integration constant k. To interpret that constant, we note that because the simplified model (13) is equidimensional, all lengthscales like k in its solution are proportional to the initial thickness a. So $k = k_1 a$, and we find that $k_1 = 2.53$ by fitting the numerical solution of (13) for $a = 1$ to (14). Microphysics therefore affects the outer solution, and so Θ, only through the thickness a seen at the apparent contact line by the distant flow. For problem (12), a is an effective thickness analogous to the displacement thickness in boundary-layer theory. (We digress to note that since $k \propto a$, the series (14) implies that $\hat{H}$ does not approach a limit as $a \to 0$; so we must take $a \neq 0$, as in (13c).) Lastly, we find k for problem (12) which includes the disjoining force.

Figure 4 shows the value of k obtained by fitting the numerical solution of the inner problem (12) to the first 4 terms of the asymptotic series (14). The figure includes the range of f common in applications, and it shows that k varies by only a factor of two

in practice. Because $k = 2.53a$, the effective initial thickness a varies between about 2 and 4. The figure shows that Θ is insensitive to microphysical detail.

From the leading term in (14), we see that $\hat{H}_x \sim \{4\ln(x/k)\}^{1/4}$; the slope does not attain a limit at the outer edge of this region since the inner evaporation rate does not vanish. As we know from (10*b*) that H_x attains a limit at infinity, we must now include the decrease in evaporation rate occurring in the large-scale outer region.

6. The outer adjustment region

To begin, we estimate the outer film thickness. The defining property of this region is that both J and T fall to zero within it. However, by elimination of J between (6*a*) and (6*b*), $T = (1-\beta PH)/(1+\beta H)$. We see T can vary only if $H = O(\beta^{-1})$ so that βH does not vanish with β; the corresponding dimensional thickness H_* is of the order of the adjustment thickness scale L. We define the outer limit as $\beta \to 0$ with βH fixed.

Next, we find the scale ℓ' parallel to the wall. By (14), $\beta H \sim 1$ when $x \sim \ell' = k\ell$, where ℓ is defined by $\beta k\ell(4f\ln\ell)^{1/4} = 1$. We show below (20) that the corresponding dimensional length ℓ'_* is related to Θ by $\Theta\ell'_*/L \to 1$ for $\beta \to 0$. The outer scales normal and tangent to the wall are thus L and L/Θ, as in the phenomenological theory (Morris 2000, § 2.2).

We define outer variables $\tilde{x}$, $\tilde{H}$ and $\tilde{P}$ by

$$\tilde{x} = x/\ell', \quad \tilde{H} = \beta H, \quad \tilde{P} = \beta\ell'^2 P, \quad \text{where} \quad B\ell(4\ln\ell)^{1/4} = 1, \quad B = \beta k f^{1/4}. \tag{15a–e}$$

The definition of the scale ℓ in the previous paragraph is repeated as (15*d*, *e*). That definition implies that $\ell = O(1/\beta)$ to logarithmic accuracy so that ℓ is algebraically large in the small parameter β. Further, ℓ is determined completely by the parameter B defined by (15*e*). B is a Biot number based on the effective film thickness $H(0)$ at the contact line since $H(0) \sim f^{1/4}a$, and $a \propto k$. Next, the pressure scale in (15*c*) follows from the balance $-P \sim H_{xx}$, and the scales for x and H. We see that $P = O(\beta)$ to logarithmic accuracy, so that the outer pressure is algebraically small in β. This is consistent with the boundary condition (12*d*) imposed on the inner analysis, namely $P(\infty) = 0$.

We obtain simplified equations for $\tilde{H}$ and $\tilde{P}$ in two steps. By substituting (15) into the governing equations (7), we obtain without approximation $(\tilde{H}^3\tilde{P}_{\tilde{x}})_{\tilde{x}} = (4\ln\ell)^{-1}(1+\tilde{P}/(\beta\ell'^2))/(1+\tilde{H})$, and $-\tilde{P} = \tilde{H}_{\tilde{x}\tilde{x}} + (\ell'\beta^2)^2/\tilde{H}^3$. We then simplify these equations by taking as negligible all terms algebraically small in β. Since $\ell' \sim 1/\beta$, the effect of pressure on evaporation is negligible in the first equation, and the disjoining force is negligible in the second. Thin-film effects are therefore negligible throughout the adjustment region, as they are at the outer edge of the inner region.

Within the adjustment region, $\tilde{H}$ and $\tilde{P}$ are thus given with algebraically small error in β by

$$(\tilde{H}^3\tilde{P}_{\tilde{x}})_{\tilde{x}} = (4\ln\ell)^{-1}(1+\tilde{H})^{-1}, \quad -\tilde{P} = \tilde{H}_{\tilde{x}\tilde{x}} \quad \text{for} \quad 0 \leqslant x < \infty. \tag{16a, b}$$

The boundary conditions are $\tilde{H}_{\tilde{x}\tilde{x}}(\infty) = 0$, and a matching condition on $\tilde{H}$ as $\tilde{x} \to 0$ yet to be derived. The domain is semi-infinite since $\tilde{x}$ and $\tilde{H}$ both vanish as $\beta \to 0$ at a fixed large value of the inner coordinate x; the outer solution has an apparent contact line at $\tilde{x} = 0$ because the inner film is thin with a short horizontal scale. Problem (16) allows the existence of an apparent contact angle, for as $\tilde{x} \to \infty$,

$(\tilde{H}^3\tilde{H}_{\tilde{x}\tilde{x}\tilde{x}})_{\tilde{x}} \to -1/(4\tilde{H}\ln\ell)$, which is readily shown to admit a solution growing linearly at infinity.

The form of the outer expansion is suggested by writing the outer limit $H \sim f^{1/4}\hat{H}$ of the inner isothermal solution in terms of the outer variables (15), then using the binomial theorem for $\ell \to \infty$ with $\tilde{x}$ fixed and possibly small to show that $\tilde{H} = \tilde{x} + \tilde{x}\ln\tilde{x}/(4\ln\ell) + o(1/\ln\ell)$, at the outer edge of the inner region. This result suggests correctly that throughout the adjustment region

$$\tilde{H} = \tilde{x} + \tilde{H}_1/(\ln\ell) + o(1/\ln\ell), \quad \tilde{P} = \tilde{P}_1/(\ln\ell) + o(1/\ln\ell) \quad \text{for} \quad \beta \to 0. \quad (17a,b)$$

The coefficient functions $\tilde{H}_1, \ldots$ are independent of β.

We now consider the outer expansion (17) to leading order, i.e. $\tilde{H} \sim \tilde{x}$ and $\tilde{P} \sim 0$. These expressions clearly satisfy (16), and match to the inner solution. Throughout the adjustment region, $\tilde{H}_{\tilde{x}}$ is therefore uniform to leading order in $1/(\ln\ell)$. To explain this, we note that by (14), $H_x = O((\ln x)^{1/4})$ at the outer edge of the inner region, so that the slope there is slowly varying in x; if x is replaced by mx, where m is an arbitrary constant, $(\ln x)^{1/4}$ is unchanged to leading order in the large quantity x. The inner isothermal region thus determines Θ at leading order, as claimed at the end of § 4. However, the outer adjustment region must be analysed to find the effective value of x, namely ℓ', at which H_x is evaluated. The outer analysis is, although necessary to determine Θ, even though the details at leading order are simple.

To test the analysis, we compare the predicted evaporative mass flux J, and interface temperature T with values computed without approximation from (7). J and T are given in terms of H and P by the enthalpy balance (6*a*) and kinetic equation (6*b*). Because the outer film is thick, the pressure term in (6*b*) is negligible so that $J = T$ and, by (6*a*), $J = 1/(1+\tilde{H})$. Since $\tilde{H} = \tilde{x}$ at leading order, $J = T = 1/(1+\tilde{x})$.

Figures 5(*a*) and 5(*b*) show the evaporative mass flux J and the interface temperature T as functions of $\tilde{x} = x/\ell'$; here, ℓ' is defined by (15*a*). For the numerical solutions, the origin is taken at the apparent contact line, so that $H \sim bx + o(1)$ for $x \to \infty$. Though the inner structure near $\tilde{x} = 0$ is not visible at the scale on which the figures are plotted, the numerical solution does resolve that behaviour. Together, these figures verify that as $\beta \to 0$, J and T approach a common asymptote $1/(1+\tilde{x})$, shown as the broken curve. This establishes two points. First, the definition of ℓ' enables us to collapse numerical solutions for $\beta \to 0$ with $\tilde{x} \neq 0$. Secondly, the leading-order solution for the adjustment region describes conduction across a liquid wedge with contact angle determined by the isothermal region. At leading order, our analysis of problem (18) is thus consistent with the phenomenological model.

We now find the second-order terms in (17). At that order, the interface is perturbed by the non-uniform pressure needed to drive the outer flow. To find that perturbation, we form equations for $\tilde{H}_1$ and $\tilde{P}_1$ by substituting (17) into (16), and applying the limit $\ell \to \infty$, i.e. $\beta \to 0$. So

$$4(\tilde{x}^3\tilde{P}_{1\tilde{x}})_{\tilde{x}} = 1/(1+\tilde{x}), \quad -\tilde{P}_1 = \tilde{H}_{1\tilde{x}\tilde{x}} \quad \text{for} \quad 0 \leqslant \tilde{x} < \infty, \quad (18a,b)$$

$$H_1/(\tilde{x}\ln\tilde{x}) \to 1/4 \quad \text{as} \quad \tilde{x} \to 0, \quad (18c)$$

$$\tilde{P}_1 \to 0, \quad \text{as} \quad \tilde{x} \to \infty. \quad (18d)$$

The differential equations (18*a*, *b*) describe quasi-parallel flow in a film of known thickness $\tilde{x}$. Equation (18*a*) states that the flow rate varies with $\tilde{x}$ owing to evaporation at a known rate imposed by the enthalpy balance (6*a*), and the leading-order solution. The pressure adjusts to drive this imposed flow, and the normal stress balance (18*b*)

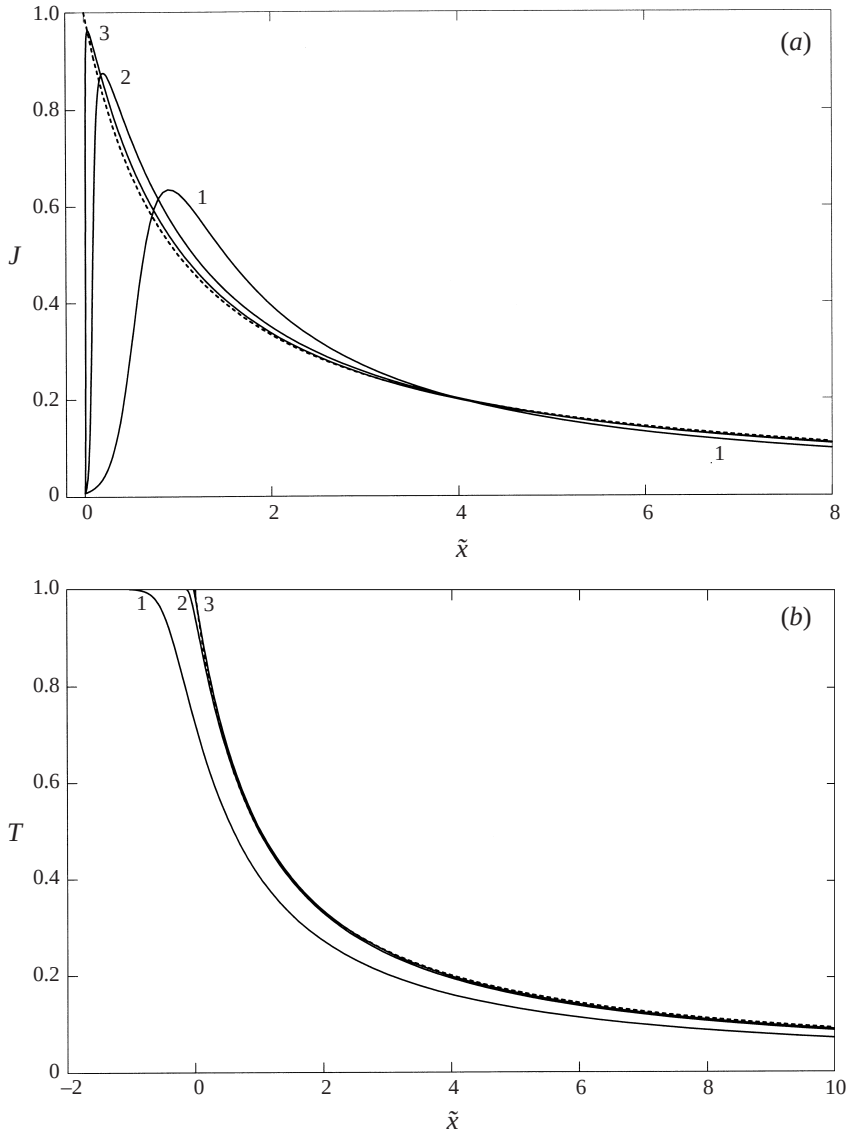

FIGURE 5. (*a*) Evaporative mass flux J and (*b*) interface temperature T as functions of $\tilde{x} = x/\ell'$ where ℓ' is defined by (15). For both figures $f = 1$, and $-\log_{10}\beta = 1, 2$ and 3 shown on the curves. Solid curves, values computed from (7). Broken curve, leading-order outer solution for $\beta \to 0$.

then determines the perturbation to the interface shape, and the correction to Θ. We find the matching condition (18*c*) by equating the inner limit $\tilde{x} \to 0$ of the outer solution (17*a*) to the outer limit of the inner solution.

We find the perturbation pressure and film thickness by integrating (18*a*, *b*), and repeatedly using the growth condition (18*c*). So $4\tilde{x}^3\tilde{P}_{1\tilde{x}} = \ln(1+\tilde{x})$

$$8\tilde{P}_1 = \ln(1+\tilde{x}^{-1}) - \tilde{x}^{-2}\ln(1+\tilde{x}) - \tilde{x}^{-1}, \tag{19a}$$

$$8\tilde{H}_{1\tilde{x}} = 3 - \tilde{x}^{-1}\ln(1+\tilde{x}) - (2+\tilde{x})\ln(1+\tilde{x}^{-1}). \tag{19b}$$

By (19*b*), $\tilde{H}_{1\tilde{x}} \to 1/4$ as $\tilde{x} \to \infty$. The slope perturbation thus varies on the same scale

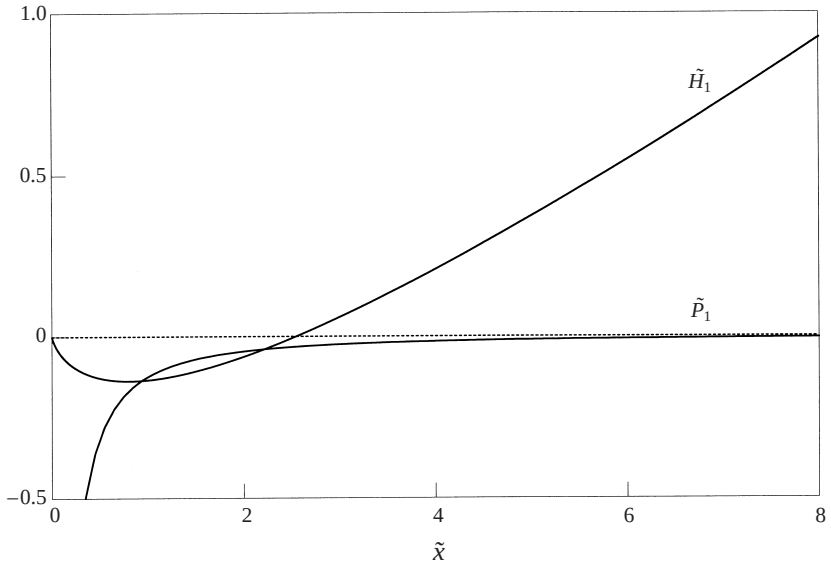

FIGURE 6. Interface perturbation and pressure within the adjustment region calculated from the second-order outer solution (19). As defined by (15) and (17), $\tilde{x} = x/(k\ell)$, $\tilde{P}_1 = P\,\beta(k\ell)^2 \ln \ell$, and $\tilde{H}_1 = (\tilde{H} - \tilde{x}) \ln \ell$.

as T. This does not contradict the phenomenological model, as that model uses only the linear interface predicted by the leading-order solution. (As an aside, we note that for arbitrary β, (10*b*) implies that H_x attains a limit when $2\beta b^5 x \gg f \ln x$, whereas the small β analysis implies that the limit is attained for $x \gg \ell'$. To show that these results are consistent, we need only use the definition (15*d*) of ℓ', and equation (20) below for b.)

Figure 6 shows the perturbation pressure $\tilde{P}_1 = P\,\beta(k\ell)^2 \ln \ell$, and film thickness $\tilde{H}_1 = (\tilde{H} - \tilde{x}) \ln \ell$ within the adjustment region. $\tilde{H}_1$ vanishes at the apparent contact line, as required by the matching condition (18*c*). The interesting feature is that $\tilde{H}_1$ changes sign; the pressure perturbation due to the outer flow thus reduces the total thickness H near the wall, but increases it for large $\tilde{x}$. This happens because $\tilde{P}_1 \to -\infty$ as $\tilde{x} \to 0$, so that the interface is drawn down near the apparent contact line, as shown by the region of negative $\tilde{H}_1$. At infinity, however, the thickness is increased since the negative pressure makes the curvature everywhere positive, so that the perturbation slope $\tilde{H}_{1\tilde{x}}$ is ultimately positive. This distortion of an otherwise linear interface affects the heat flow by changing the conduction path, as we discuss following (26).

7. Predicted contact angle

To find Θ, we determine the slope parameter b using (17), the result $\tilde{H}_{1\tilde{x}} \to 1/4$, and the definitions (15) of the outer variables. So, for $\beta \to 0$,

$$b/f^{1/4} \sim (4 \ln \ell)^{1/4}\{1 + 1/(4 \ln \ell)\}, \quad \beta b \ell' \sim 1 + 1/(4 \ln \ell). \tag{20a,b}$$

The relative error in each of these expansions is $o(1/\ln \ell)$. Equation (20*b*) follows from (20*a*), and the definition (15*d*) of ℓ. When interpreted, (20*b*) relates the dimensional length $\ell'_* = \ell' L_s$ to the adjustment thickness L; since $\ell' \sim 1/(\beta b)$ by (20*b*), and $\beta = H_s/L$ by the definition of L, it follows that $\ell'_* \sim L/\Theta$ at leading order in β. The outer lengthscale along the wall is thus L/Θ, as claimed above (15).

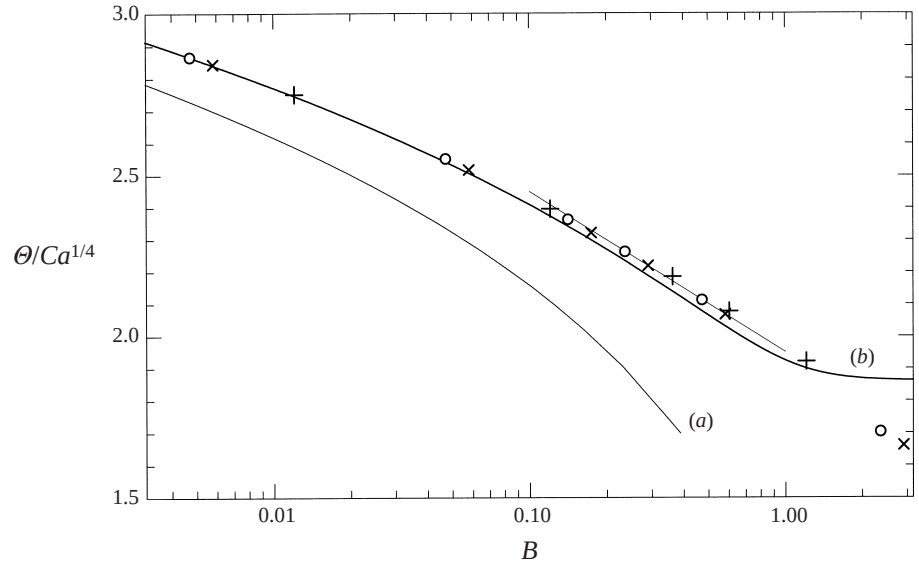

FIGURE 7. $\Theta/Ca^{1/4}$ as a function of B. Symbols, values computed without approximation from problem (7), and the definition (8) of b: +, $f = 20$; ×, $f = 1$; ○, $f = 0.05$. Line, fit (22a) to computed values; curve (a), first-order asymptotic analysis; curve (b), telescoped two-term result (21). $k(f)$ is given by figure 4. See text below (21) for discussion, and definitions of B and Ca.

Equation (20a) expresses the slope parameter as the sum of two effects. The first, or leading-order, term in braces is the contribution of the inner isothermal region. The second, and smaller, term represents the change in slope across the outer adjustment region. The binomial theorem can be used to combine those terms to show that $b/f^{1/4} = \sqrt[4]{4\ln(\mathrm{e}\ell)} + o(1)$, where $\mathrm{e} = \exp 1$. By substituting this expression into (8b), we find that for $\beta \to 0$

$$\Theta = \sqrt[4]{12Ca\ln(\mathrm{e}\ell)} + o(1), \quad \text{here} \quad B\ell(4\ln\ell)^{1/4} = 1. \tag{21a,b}$$

Equation (15d) for ℓ is repeated as (21b). The Biot number $B = \beta k f^{1/4}$, as defined by (15e). The parameters β, f and Ca are defined in table 1; in particular, the capillary number $Ca = \mu_\ell V_\ell/\sigma$ where the velocity scale V_ℓ, as defined by (4a). We note that because the interface slope is assumed small in writing the governing equations (1), our analysis holds if $Ca \to 0$.

Though we shall see that equation (21) accurately predicts Θ, it has a more significant implication; contact angles for different values of β, f and Ca should lie on a single curve when $\Theta/Ca^{1/4}$ is plotted against B. In figure 7, we test this prediction. Symbols denote values computed without approximation for $f = 0.05, 1$ and $f = 20$, and values of β between about 0.0003 and 0.3. These values include the range typical of applications using non-metallic liquids.

Figure 7 shows that the scaling suggested by (21) collapses the numerical results even for B of order unity. This empirical result implies that, as predicted by our analysis, the only effect of microphysics on Θ is to impose the effective film thickness used to define B. Further, we see that $\Theta/Ca^{1/4}$ depends only weakly on B. In the examples $0.1 < B < 1.1$, and the figure shows that over this range

$$\Theta/Ca^{1/4} = 1.95 - \tfrac{1}{2}\log_{10} B, \quad \text{so} \quad \Theta = 2.2Ca^{1/4} \tag{22a,b}$$

with an error less than $\pm 15\%$ in practice. Equation (22b) expresses the apparent contact angle as a function of a single parameter Ca depending only on well-known

macrophysical properties. This important result implies that in a plot of Θ against Ca, the entire dependence of Θ on microphysics amounts to a modest scatter in that plot; indeed, we shall see in § 10 that the experimental error in measuring Θ is comparable with that in the simple relation (22*b*). Though Stephan (1992, figure 5.17) concludes that Θ is insensitive to the value of A, no one before has used that insensitivity to derive a simple formula for Θ.

In addition to suggesting the formula (22), the asymptotic result (21) also predicts Θ accurately. In figure 7, curves (*a*) and (*b*) show, respectively, the one-term and two-term predictions of the asymptotic analysis. The one-term prediction includes only the contribution of the inner isothermal region to $\Theta/Ca^{1/4}$; it is obtained by setting '$e = 1$' in (21). The two-term prediction is given by (21) as displayed, and includes the additional contribution to Θ from the adjustment region. Curve (*b*) fits the numerical results nicely, so that the second-order analysis is accurate for values of the parameters occurring in practice. Curve (*a*) shows that the increase in slope across the thickness region is significant in examples like that of Stephan & Busse, for which $B = 1.1$; however for 8 of Kim's 11 experiments on octane, table 2 shows that $B < 0.5$. Even the one-term analysis represented by curve (*a*) then predicts Θ to within 30%. The one-term analysis becomes increasingly accurate to the left-hand side of the figure as $B \to 0$.

The only equation comparable to (21) is that derived by Hocking (1995) following a heuristic discussion by Anderson & Davis (1995, equation 20). Hocking's analysis describes a slightly different physical situation, as he takes the fluid as partially rather than perfectly wetting; thus, the static contact angle $\Theta_0 \neq 0$. However, he does not include the thermodynamic effects of the short-range forces that create Θ_0; since those forces set a minimum scale, and so prevent the occurrence of a velocity singularity, in their absence Hocking must impose a scale instead. He does that by using a slip boundary condition in which the tangential velocity u_0 at $y = 0$ satisfies $u_0 = \mathscr{L}(\partial u/\partial y)_0$, where $\mathscr{L}$ is the constant slip length. In our notation, Hocking's (14) states that $\Theta^4 \sim \Theta_0^4 + 12\,Ca \ln\{\Theta_0/(2\Theta\beta_{\mathscr{L}})\}$ for vanishing Biot number $\beta_{\mathscr{L}} = h\mathscr{L}/K_\ell$. (Our $\beta_{\mathscr{L}}$ is the ratio of Hocking's 'β' to his 'K'; as stated following his (6), his analysis is for '$K \gg \beta$', i.e. for $\beta_{\mathscr{L}} \to 0$.) This prediction shares with our (21) a common scaling $\Theta \sim Ca^{1/4}$ for $\Theta \gg \Theta_0$, and a common functional form for the dependence on microphysics; only the argument of the logarithm differs. Hocking does not derive a simplified result like (22*b*).

8. Simplified model of the evaporating meniscus

To explain why the slip and wetting models predict similar results for Θ, we formulate a purely hydrodynamic model of the evaporating meniscus. This model has an inner and outer structure, the inner and outer problems being (13) and (16). To construct the model, we note that in both (13) and (16), the effect of pressure on evaporation kinetics is negligible; so we use the kinetic equation $J = h(T - T_o)/Q$ given below (4). Similarly, we take the disjoining force as negligible; so we take the domain as semi-infinite, and impose a dimensional film thickness a_* at the origin. We define length and pressure scales by $L_s' = a_*/Ca^{1/4}$ and $P_s' = 3\mu_\ell V_\ell L_s'^2/a_*^3$; so L_s' is the horizontal scale on which the capillary pressure balances the pressure difference P_s' needed to drive the evaporatively induced flow in a film of thickness a_*. We then define the dimensionless film thickness H, distance x, and pressure P by $H = H_*/a$, $x = x_*/L_s'$ and $P = (P_* - P_o)/P_s'$; the dimensionless temperature and evaporative mass flux are as defined by (5).

In this hydrodynamic model, the dimensionless pressure P, film thickness H, interface temperature T and evaporative mass flux J satisfy $(H^3P_x)_x = J$, $J = T$, $(1-T)/H = B'J$, and $-P = H_{xx}$. By elimination of J and T, we find that P and H satisfy

$$(H^3P_x)_x = 1/(1+B'H), \quad H_{xx} = -P \quad \text{for} \quad 0 < x < \infty, \tag{23a,b}$$

$$H = 1, \quad H_x = 0 = P_x \quad \text{at} \quad x = 0, \tag{23c,d}$$

$$P \to 0 \quad \text{as} \quad x \to \infty. \tag{23e}$$

Here, the Biot number $B' = ha_*/K_\ell$, which is proportional to the quantity B used in § 7. Problem (23) has physical significance only if $B' \to 0$, for only then can microphysics be parameterized by a lengthscale.

These equations differ from a similar system used for thick evaporating films by Anderson & Davis (1995, equation 9) in one essential; we assume a no-slip boundary condition in (23*a*) where Anderson & Davis allow slip. However, there is no reason to believe that slip is essential to the evaporating meniscus. Thompson & Troian (1997) have used molecular dynamics to compute the slip length Λ as a function of strain rate in a Couette flow. Though they find that Λ depends on the ratio of the bond lengths in the liquid and solid, application of their results to the evaporating meniscus suggests that $\Lambda \sim H_e$, the thickness of the equilibrium film. As the liquid in that equilibrium film is stationary relative to the wall, slip seems unlikely to be physically significant. Anderson & Davis use it as a device to prevent a velocity singularity; we achieve that end instead by imposing a non-zero film thickness at the origin, and we determine that length by the analysis in §§ 5 and 6.

We can now explain the fourth-root dependence. Because the solution of (23) depends on the single parameter B', we see that $\lim_{x\to\infty} H_x = \mathrm{fn}(B')$, and since $L_s' = a_*/Ca^{1/4}$, $\Theta = Ca^{1/4}\mathrm{fn}(B')$. Though the function $\mathrm{fn}(B')$ does not approach a limit as $B' \to 0$, that does not affect the fourth-root dependence on Ca since Ca and B' are independent parameters. Because the normal velocity is imposed by evaporation rather than the tangential velocity, a fourth-root dependence occurs here instead of the cube root familiar from Tanner's rule for isothermal spreading.

A thermodynamically complete analysis of an evaporating, partially wetting system would be of interest, as physical reasoning suggests the coefficient of $Ca^{1/4}$ might be increased by the short-range forces creating the static contact angle. The existence of a non-zero static contact angle is known to require the interface to be attracted to the wall over a range of film thicknesses; see Wong, Morris & Radke (1992), and references there. Because we have seen that a repulsive force between the interface and wall impedes evaporation from the thin inner film, an attractive force should enhance evaporation. This logic shows that although (23) requires $\Theta \sim Ca^{1/4}$, the numerical coefficient should increase with Θ_0. Though Hocking's equation (14) predicts such an increase, its cause is unclear to me as his model contains no thermodynamics.

9. Heat flow

We now consider the heat flow, as part of our analysis of Kim's experiments requires us to infer ΔT from the measured evaporation rate. The dimensional heat flow q_* across the interval $(-\infty, x)$ is given by $\Theta q_*/(K_\ell \Delta T) = \beta b\ell'(4\ln\ell)\tilde{H}^3\tilde{P}_{\tilde{x}}$; here, we have used (9) and the identity $H^3P_x = (4f\ell'\ln\ell)\tilde{H}^3\tilde{P}_{\tilde{x}}$. To find q_*, we need the

matching condition

$$\lim_{\tilde{x}\to 0} \tilde{H}^3 \tilde{P}_{\tilde{x}} = 0, \tag{24}$$

which follows from the equation immediately preceding it, because at the outer edge of the inner region $H^3 P_x$ is independent of β, while $(4f\ell' \ln \ell)$ is algebraically large in β. Equation (24) states that the evaporation from the inner region is negligible compared with that from the outer region, as we expect from the numerical solutions discussed following figure 3.

To find q_*, we substitute for $\tilde{H}$ from (17*a*) on the right-hand side of the governing equation (16*a*), use the binomial theorem, and then integrate (by parts, where appropriate) to find $\tilde{H}^3 \tilde{P}_{\tilde{x}}$. The integration constant is zero by (18*c*) and the matching condition (24). So for $\beta \to 0$,

$$\frac{\Theta q_*}{K_\ell \Delta T} = \beta b \ell' \left\{ \left(1 - \frac{1}{\ln \ell} \tilde{H}_{1\tilde{x}} \right) \ln(1+\tilde{x}) + \frac{1}{\ln \ell} \left(\frac{\tilde{H}_1}{1+\tilde{x}} - \int_0^{\tilde{x}} \tilde{P}_1 \ln(1+\tilde{x})\, \mathrm{d}\tilde{x} \right) \right\} + o\left(\frac{1}{\ln \ell} \right). \tag{25}$$

The terms have been grouped here to promote interpretation.

To interpret (25), we first study its behaviour for $\tilde{x} \to \infty$. The integral then approaches the limit $\int_0^\infty \tilde{P}_1 \ln(1+\tilde{x})\, \mathrm{d}\tilde{x} = \frac{1}{8}(1 - \frac{1}{3}\pi^2)$, while $\tilde{H}_1 \sim \tilde{x}/4$ by (20*b*), so that

$$\Theta q_*/(K_\ell \Delta T) \sim \ln \tilde{x} + c_1/(\ln \ell) + \cdots. \tag{26}$$

Here, $c_1 = \frac{1}{8}(1 + \frac{1}{3}\pi^2)$, and we have used (20*b*), i.e. $\beta b \ell' \sim 1 + 1/(4 \ln \ell)$, to simplify the coefficient of $\ln \tilde{x}$. As defined by (15), $\tilde{x} = x/\ell'$ and $\ell' = k\ell$, where k is given by figure 4. The error in (26) is $o(1)$ in $\tilde{x}$, and $o(1/\ln \ell)$ in ℓ. Because we have used (20*b*) here, the value of Θ on the left-hand side is that given by the second-order equation (21*a*).

We now interpret equation (26). At first order, the contact region imposes a lengthscale ℓ' on which the contact line singularity is resolved. The notation $x \to \infty$, which is ambiguous in (10) unless β and f are both $O(1)$, now has a precise meaning even for $\beta \to 0$; it is that $x/\ell' \to \infty$. By the discussion following (20*b*), $\tilde{x} \sim \Theta x_*/L$, which expresses $\tilde{x}$ in terms of the adjustment thickness and the dimensional position. Next, interface distortion within the adjustment region has two mutually opposing effects on the heat flow. It increases the conduction path for large x, but decreases it near the apparent contact line. The first effect enters (26) through the value of Θ, and the second, through the positive term $c_1/(\ln \ell)$. The overall effect is to reduce q_* since distortion for large x affects q_* through the multiplier Θ, while distortion near the contact line merely determines the additive constant c_1. This suggests that we should predict heat flows by combining the first-order analysis for q_* with the accurate second-order result for Θ; this is effectively the path followed by Morris (2000), as Θ is computed there without approximation.

At leading order, there is a simple expression giving $q_*(\tilde{x})$ for all $\tilde{x}$ because the outer interface is then linear everywhere. For $\ln \ell \to \infty$, (20*b*) implies that $\beta b \ell' \to 1$. By (25), $\Theta q_*/(K_\ell \Delta T) = \ln(1+\tilde{x}) + o(1)$ for $0 \leqslant \tilde{x} < \infty$. We express this in terms of the dimensional coordinate x_*, Θ and the adjustment thickness L by using the asymptotic relation $\tilde{x} \sim \Theta x_*/L$ given above. So

$$\Theta q_*/(K_\ell \Delta T) = \ln(1 + \Theta x_*/L) + o(1). \tag{27}$$

The origin for x_* is at the apparent contact line, because the outer solution (17a) shows that at leading order the outer film thickness $\tilde{H} = \tilde{x}$.

Equation (27) is identical with the prediction of the phenomenological model, in which the temperature is found by solving the steady conduction equation subject to Newton's law on a linear interface with given contact angle. The two analyses of heat flow have the same physical basis, since we have seen that the interface is linear on the scale at which heat flow occurs, and conversely that by (24), there is negligible heat flow in the region where Θ is established. Further, Newton's law holds in the present analysis of the heat flow because the effect of pressure on evaporation is negligible within the thick outer film. By elimination of J between (6a) and (6b), the film thickness and interface temperature then satisfy $\beta T + (T-1)/H = 0$, which is the form taken by Newton's law for $\Theta \to 0$, when $\partial T/\partial n = (T-1)/H$. Equation (27) can thus be derived by solving the simplified form of the phenomenological model appropriate to a thin film on an isothermal substrate, namely

$$T_{yy} = 0, \quad \text{for} \quad 0 < y < \beta x, \tag{28a}$$

$$T_y + \beta T = 0, \quad \text{at} \quad y = bx, \tag{28b}$$

$$T = 1, \quad \text{at} \quad y = 0. \tag{28c}$$

In problem (28) only, we use T both for the temperature at the interface, and for that within the liquid.

Figure 8 shows the heat flow q_* as a function of $\Theta x_*/L$ for $f = 1$, and two values of β representative of those in table 1. Throughout this work, x_* is dimensional and the adjustment thickness $L = K_\ell/h$, as defined in § 1. The heavy curve shows the prediction (27); for that curve, Θ is found from the accurate result (21). Light curves show values computed without approximation from (7), (8) and (9). Broken lines show the second-order asymptote (26). By comparing the heavy and light curves, we see that if Θ is calculated from (21), equation (27) predicts the heat flow accurately even for $\beta = 0.1$ if $\Theta x_*/L > 5$. For $\beta = 0.01$, the prediction is accurate if $\Theta x_*/L > 1$. This use of (27) combines a second-order result for Θ with a first-order result for q_*; this is admissable, as q_* is determined for large x chiefly by Θ rather than by details near the vertex of the wedge. The heat flow is thus predicted accurately in practice by combining the phenomenological model with equation (21) for Θ. Morris (2000, figures 7, 8 and 10) gives a detailed comparison of the phenomenological model with the simulation of Stephan & Busse (1992); that comparison includes the effect of substrate conduction.

For use below, we note in Kim's experiments on octane, L/Θ is between 5 and 50 μm. Since the horizontal extent is much larger than that, we see from figure 8 that the phenomenological model can be applied to his experiments.

10. Comparison with existing experiments

Kim (1994, figures 5.5–5.20) gives film profiles measured by interferometry for two liquids, octane and R113 ($C_2F_3Cl_3$) evaporating from a superheated substrate of Si with a oxidized surface layer of thickness 2–3 nm. The liquid evaporates into a mixture of air and the vapour phase, so that the liquid and gas are not chemically identical. As we note in § 1, though Kim and Kim & Wayner (1996) infer local values of the slope from Kim's measured profiles, they do not report values of Θ; the values given here seem to be the first published for evaporating systems.

To find Θ from Kim's measured profiles, I used the approach in § 3. I numerically

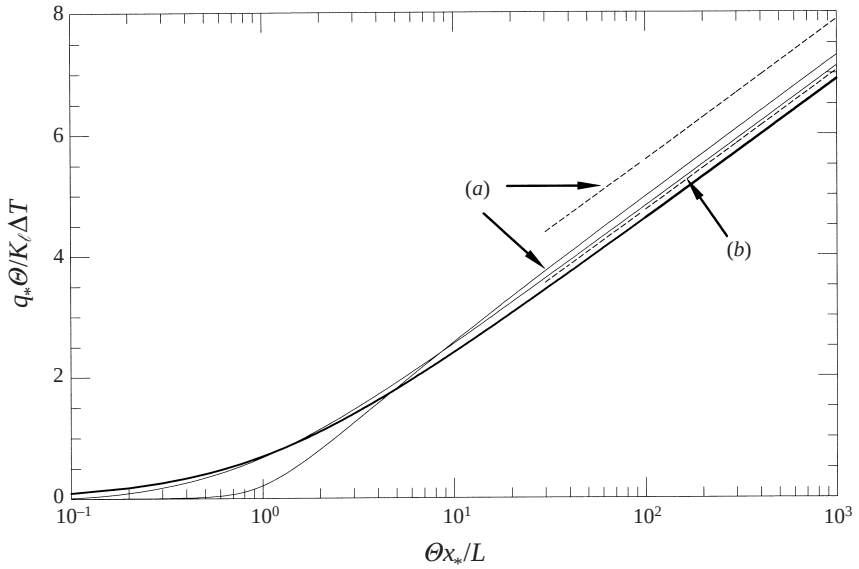

FIGURE 8. Heat flow $q_*\Theta/(K_\ell\Delta T)$ as a function of position $\Theta x_*/L = \beta bx$ within the contact region, where $L = K_\ell/h$ as defined in § 1. Heavy curve, prediction (27). Light curves, computed without approximation from (7) and (9). Broken lines, asymptotic relation (26). For (*a*), $\beta = 0.1$ and $f = 1$; for (*b*), $\beta = 0.01$ and $f = 1$.

differentiated the dimensional thickness H_*, then plotted H_{x*}^2 against H_*. As we discuss above (8), the constant curvature part of the interface becomes a line in the (H_{x*}^2, H_*)-plane; its slope is proportional to the curvature, and the intercept determines Θ^2. The advantage of the new method is that the constant-curvature region is evident in the (H_{x*}^2, H_*)-plane; such plots show that in Kim's experimental profiles, the curvature becomes constant only at film thicknesses exceeding 0.2–0.3 μm. I discarded data from the region of variable curvature, and fitted a line to the rest by the least squares method. The new method allows Θ to found repeatably, and without using the theory to be tested.

Values of Θ thus found differ from those given by Kim & Wayner (1996, figure 6). Those authors vary the dispersion constant A to fit the computed and measured profiles, and then compute the slope at specific film thicknesses (either 0.02 or 0.04 μm); they call the result the 'apparent contact angle' for a specific thickness (Kim & Wayner 1996, equation 14). Their values have no relation to the prediction (21) as the thicknesses $\sim 0.02\,\mu$m at which they compute the angle are about a tenth that at which the curvature becomes uniform in the experiments. Unlike the angle defined by (8), the quantity computed by them cannot be used with equation (27) to find heat flows.

Next, we discuss the method by which Kim measured ΔT. In the experiments, ΔT is typically less than a millikelvin, and is too small to be measured directly. Instead, Kim measures the thickness H_e of the equilibrium film by ellipsometry, then infers ΔT from the condition of thermodynamic equilibrium. However, he uses equation (11) of DasGupta *et al.* (1993) to make the inference. I believe that equation to be incorrect as we discuss above (2). To infer ΔT from Kim's measurements, we use (3) and (1*d*) to show that

$$(T_w - T_\infty)/T_\infty = (A/H_e^3 - \Delta P)/(\rho_\ell Q). \tag{29}$$

On the left-hand side of (29) we have replaced T_o in the denominator by T_∞, because $T_\infty \doteqdot T_o$ by (2*b*). Equation (29) expresses the applied temperature difference ΔT in terms of T_∞, the measured equilibrium thickness H_e, the pressure difference $\Delta P = P_a - P_{\ell\infty}$ across the interface at infinity, and thermodynamic properties; they are the dispersion constant A, liquid density ρ_ℓ and latent heat Q. As we state above figure 1, material properties are evaluated at the wall temperature T_w. Though the prediction (21) implies that Θ depends only weakly on A, the relation (29) between ΔT and H_e depends linearly on A. Use of (29) thus introduces a stronger dependence on A than that existing in the physical problem.

To find ΔT from Kim's measurements of H_e, I assume A to be independent of T and use values determined experimentally for the isothermal meniscus by Kim. Though T_w varies from 300 K to 360 K in Kim's experiments, my procedure is justified as A is insensitive to temperature. Müller-Buschbaum, Tolan & Press (1994, table 1) show experimentally that for CCl_4 on Si–SiO_2, A varies from (21 ± 5) zJ at 308 K to (20 ± 4) zJ at 318 K. (A zeptojoule is 10^{-21} J.) These values suggest A may decrease weakly with increasing T_w, but that to a first approximation, A is constant. This conclusion is consistent with the dependence of A on T_w inferred by Reyes & Wayner (1996, figure 2) from an empirical relation between A and surface energies. By contrast, Kim varies A to fit the computed and measured film profiles, and since T_w varies between experiments, he finds A as a function of T_w. I did not use that method as it predicts A to vary with T_w more strongly than expected from the citations above.

I use the following values for A; for octane on Si–SiO_2, $A = 0.03$ zJ (Kim 1994, table 5.2) and for R113 on Si–SiO_2, $A = 0.15$ zJ (DasGupta *et al.* 1993, table 3). The value for octane is smaller than other estimates for isothermal systems; Levinson *et al.* (1993) find experimentally that $A = 0.9$ zJ for octane on Si–SiO_2, and Truong & Wayner (1987) predict theoretically that $A = 0.4$ zJ. Kim (1994, p62) attributes the discrepancy to water adsorbed on the silicon.

I tested the choice $A = 0.03$ zJ for octane as follows. For one case, $T_w = 303$ K, Kim measured the rate at which the level in the liquid reservoir fell, and inferred the evaporation rate $\Psi_* = 0.880$ nl s^{-1} (Kim 1994, table 5.19); the corresponding heat flow $\rho_\ell Q \Psi_* = 0.232$ mW. From this, and the length 62.8 mm of the contact line found from Kim's figure 3.2, we infer that the heat flow per unit length of contact line $q_* = 3.68$ mW m^{-1}. To find ΔT from q_*, I assumed an isothermal substrate, and solved the conduction equation for the thin film subject to Newton's law at the parabolic interface $H_* = \Theta x_* + x_*^2/(2R)$ to show that

$$\Theta q_*/(K_\ell \Delta T) = \frac{2}{\sqrt{1-\alpha}} \tanh^{-1} \sqrt{1-\alpha}. \tag{30}$$

Here, $\alpha = 2L/(\Theta^2 R)$ is twice the ratio of the adjustment thickness L to the thickness $\Theta^2 R$ at which the quadratic term in the equation for H_* balances the linear term; the flux then switches from a slow $1/x_*$ decay to a faster $1/x_*^2$ decay, so that the heat flow approaches a limit at infinity. (We treat large-scale curvature in more detail in a subsequent paper.)

The conduction model is applicable to the experiments for the following reasons. First, conditions (3*a–c*) of Morris (2000) must be satisfied if we are to use a contact angle to compute heat flows; these conditions involve only measurable quantities, and can be shown to hold for the experiment in question. Secondly, for the conduction model to give the heat flow accurately, the extent X_* of the meniscus must be great

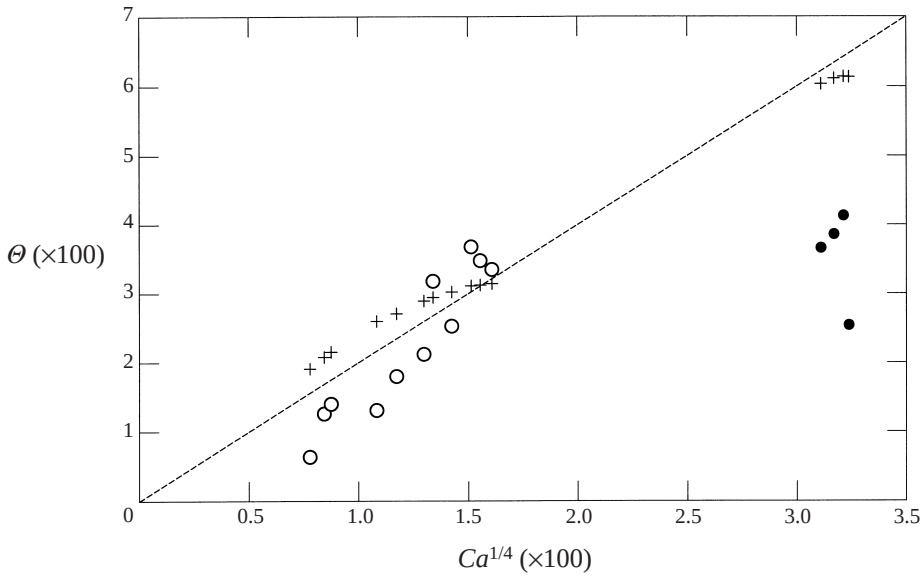

FIGURE 9. Measured and predicted contact angles. ○, ●, experimental values inferred from profiles measured by Kim (1994) for octane, and R113, respectively; +, calculated from (22*a*); broken line, $\Theta = 2Ca^{1/4}$, least-squares fit to calculated values. See table 2 for experimental values.

enough for the model to apply over a large region; we saw in the discussion of figure 8 that this requires $X_* > L/\Theta$, which is satisfied in the experiments.

From my fit to the measured profile given as figure 5.8 of Kim (1994), $\Theta = 0.014$ and $R = 1.66\,\text{mm}$. From tables of material properties we find $K_\ell = 0.13\,\text{W m}^{-1}\,\text{K}^{-1}$, and the heat transfer coefficient $h = 0.259\,\text{MW m}^{-2}\,\text{K}^{-1}$, so that $L = 0.50\,\mu\text{m}$. Equation (30) can now be solved for $\Delta T \doteqdot 0.30\,\text{mK}$. That is ~ 1.2 times the value of 0.24 mK estimated from Kim's measured equilibrium film thickness of 5.2 nm, and the agreement supports the use of the value given above for A. Of course, the very close agreement is not significant; in the conduction calculation, I assume an isothermal substrate, but equation (33) of Morris (2000) can be used to show that is only a fair approximation here. The significant point is that the alternative choice $A = 0.9\,\text{zJ}$ for octane would lead to estimates of ΔT differing by a factor ~ 30. We also see that ΔT can be found by measuring the volumetric evaporation rate, then using conduction theory.

Figure 9 shows Θ as a function of the capillary number defined in table 1. Circles, both open and closed, denote experimental values inferred from Kim's measured profiles, while plus signs denote values predicted by (22*a*); the experimental values are also given in table 2. The broken line $\Theta = 2Ca^{1/4}$ is fitted by least squares to the predicted values; the coefficient 2 lies within the range stated in the abstract of this paper. The figure shows adequate agreement between the experimental and predicted values. The two agree to within $\pm 40\%$ for 9 of the 15 experiments, with much of the error originating in Kim's four profiles for R133. Those profiles are visibly rough, and there is considerable scatter in the local values of the slope used to infer Θ; this is especially so of the profiles giving the greatest and least values for R113. Though the values for R113 worsen the quantitative agreement between theory and experiment, they are included to stress that two liquids with quite different dispersion constants have apparent contact angles obeying (22) with fair accuracy. The scatter $\sim \pm 25\%$ in

Fluid	T_w(K)	$10^8 Ca$	$100\Theta_e$	100β	$f/10$	10ϵ	B	Relative error
Octane	301	0.37	0.64	1	0.7	0.7	0.1	1.0
	302	0.51	1.3	1	0.7	0.5	0.09	0.5
	303	0.59	1.4	1	0.7	0.6	0.09	0.4
	312	1.4	1.3	1	0.8	0.4	0.1	0.7
	320	1.9	1.8	2	1	0.7	0.2	0.4
	329	2.8	2.2	3	1	0.8	0.3	0.3
	333	3.2	3.2	3	1	0.8	0.3	0.08
	338	4.1	2.5	4	2	0.8	0.5	0.2
	347	5.2	3.7	5	2	1	0.6	0.2
	353	5.9	3.5	6	2	2	0.8	0.1
Octane	359	6.7	3.4	7	3	3	1	0.06
R113	302	93	3.7	10	1	0.08	1.0	0.5
	304	101	3.9	10	1	0.09	1.1	0.5
	306	106	4.1	10	1	0.3	1.2	0.4
R113	308	110	2.5	10	1	0.5	1.3	0.8

TABLE 2. Parameter values for figure 9. In the last column, the relative error gives the difference between the fit (22*a*) to the computed values Θ_c and the experimental value Θ_e; it is defined as $2|\Theta_e - \Theta_c|/(\Theta_e + \Theta_c)$

.

the values for R113 gives a rough estimate for the random error in the experimental values; the random error for octane is comparable, as we see from the two measured values with $Ca^{1/4} \sim 0.014$.

One of the main points in this paper is the precise definition (8) of Θ, with its underlying idea that Θ is defined by a limit. It must be ensured experimentally that the measured angles are independent of the large-scale curvature. Experiments to date suffer from the lack of this idea. For the three points for octane with $\Theta \doteqdot 0.04$, table 2 shows that $0.1 < \epsilon < 0.3$. We see from figure 2 that the measured values of Θ depend on ϵ, and consequently may be only two-thirds the true limiting value. More experiments are needed at smaller values of ϵ to test the theory.

11. Discussion

Though it has long been known that the evaporating meniscus exhibits an apparent contact angle, our asymptotic analysis establishes that this angle is fundamental to computing the heat flow. It also gives formulae for the heat flow and contact angle. The analysis exploits the separation of scales existing for vanishingly small Biot number based on the evaporative heat transfer coefficient, liquid conductivity and thickness of the equilibrium film. We show that the apparent contact angle Θ is then determined within a small-scale inner region, within which a negligible fraction of the total evaporation occurs. The heat flow occurs at larger scales in a geometry determined by Θ, and is determined by solving the steady conduction equation for the liquid wedge subtending an angle Θ. On the outer phase interface, Newton's law of cooling holds, i.e. $K_\ell \partial T/\partial n + h(T - T_\infty) = 0$, where n is distance into the vapour. We call this outer problem the phenomenological, or conduction, model for the heat flow. Our analysis of the inner region gives a formula for Θ; see equation (21). We show that the angles predicted by that formula agree in practice to within a few per cent with values computed without approximation from the theory of the evaporating meniscus; the predicted values of Θ also agree adequately with the experiments of

Kim (1994). This paper thus establishes the claims made in the last paragraph of Morris (2000).

The advantage of this approach for predicting heat flows is neatly illustrated by our comparison in §10 of predicted values of Θ with values inferred from Kim's measured profiles. As part of that comparison, we require the applied temperature difference ΔT. Because the conditions for validity of the conduction model for heat flow can be expressed purely in terms of phenomenological variables, including Θ, we were able to justify using that model to infer ΔT from Kim's measured evaporation rate. Unlike the method used by Kim to infer ΔT, our method is independent of wetting physics.

The present treatment of heat flow differs in principle from that in Morris (2000) because here the conduction model is derived by asymptotic analysis for $\beta \to 0$ of a complete model of the contact region; there, by contrast, the conduction model is justified by showing that it provides a self-consistent picture of the contact region if

$$\mathscr{P} = \rho_v v_\ell / (\rho_\ell C L \Theta^2) \ll 1, \quad Ca/\Theta^4 \ll 1, \tag{31a,b}$$

and $\Theta \Lambda / L \ll 1$ (Morris 2000, equations 3*a–c*). Here, Λ is the molecular free path within the vapour, and L is the adjustment scale. The first inequality ensures that the effect of liquid pressure on evaporation kinetics is negligible; the second, that the interface slope is uniform at the scale L/Θ; and the third, that pressure differences within the vapour phase do not affect evaporation kinetics.

We now show that the inequalities (31*a*, *b*) are satisfied for $\beta \to 0$; the conduction model is thus equivalent to one part of the present asymptotic analysis, as claimed by Morris (2000, p. 87). (The third inequality cannot be derived from problem 7, as pressure differences within the gas are assumed negligible in deriving problem 7.) First, the parameter $\mathscr{P}$ can be expressed in terms of the parameters in the present theory by using (21) to eliminate Θ; so $\mathscr{P}^2 = \beta^2 f/(36\lambda^2 \ln \mathrm{e}\ell)$. By elimination of f between this relation and the definition (15*d*) of ℓ, we find that $\mathscr{P} = 1/(12\lambda\beta\ell'^2 \ln \ell)$; here, we have used $\ln \mathrm{e}\ell \sim \ln \ell$. The effect of pressure on kinetics is thus negligible according to (31*a*) if $\beta\ell'^2 \ln \ell \gg 1$. This condition is equivalent to the scalings given in §6, because in the unnumbered equation opening the paragraph above (16), the effect of pressure on evaporation is represented by the term $\tilde{P}/(\beta\ell'^2)$. This is $\sim 1/(\beta\ell'^2 \ln \ell)$ because $\tilde{P} \sim 1/\ln \ell$ by (17*b*). The condition (31*a*) is thus equivalent to the scalings in §6. Secondly, the inequality (31*b*) is plainly satisfied for $\beta \to 0$ by (21*a*). The inequalities (31*a*, *b*) are satisfied for $\beta \to 0$, as claimed.

Here, we have analysed in detail only the case $\epsilon = 0$ for which the large-scale curvature is vanishingly small compared with that in the contact region. The limit $\epsilon \to 0$ is singular in two different ways. First, if the interface is stationary relative to the wall, the singularity is weak; it does not affect the contact angle, but there is a significant effect on the heat flow in the case $\epsilon \downarrow 0$, in which the interface is concave up. To understand the effect, note that for $\epsilon > 0$, (7*b*, *c*) require that $H \sim \frac{1}{2}\epsilon x^2$ as $x \to \infty$. The mass balance (7*a*) then implies that $(H^3 P_x)_x = O(1/(\epsilon x^2))$ at infinity. The heat flux thus decays as x^{-2}, and is integrable at infinity because the film thickness increases faster than x. The limit $\epsilon \downarrow 0$ is singular because the x^{-2} decay in the heat flux is replaced for $\epsilon = 0$ by a slower x^{-1} decay which is not integrable at infinity. By incorporating the small positive curvature when the interface is concave up, a total heat flow can be associated with the contact region. Heat pipes are efficacious because that heat flow grows indefinitely as $\epsilon \to 0$. A subsequent paper will describe the heat flow calculation for the weakly curved interface, and verify the predictions

of the local analysis against a complete solution for the heat flow across the meniscus in a channel.

Secondly, the singularity is even stronger when there is spreading; then, as we have seen in §1, even the contact angle depends on ϵ because $\lim_{x\to\infty}\lim_{\epsilon\to 0} H_x$ does not exist. The problem is obtained from (7) by modifying the mass balance to include boundary motion. Relative to axes moving with the contact line the mass balance then becomes $(H^3P_x)_x = \mathscr{U}H_x + f(1+P)/(1+\beta H)$, where the positive parameter $\mathscr{U}$ is a dimensionless measure of the boundary velocity in the x-direction. The mass flow $\mathscr{U}H$ due to boundary motion increases with film thickness H more strongly than that due to evaporation, and the interesting problem is that for which $\mathscr{U}\to 0$ so that the boundary motion affects the interface only far from the contact line. We anticipate a structure in which evaporation establishes one contact angle Θ_e at small scales, while the boundary motion alters this slope at larger scales to a second value Θ_b. Either angle might control the heat flow, depending on the value of ϵ. This problem will be analysed in a subsequent paper.

I thank Enrique Ramé, Howard Stone, Peter Wayner and the referees for helpful comments; and members of the Radke research group in the Chemical Engineering Department at Berkeley for many illuminating discussions.

Appendix A. On thermocapillary stresses

We show that for $\beta\to 0$, thermocapillary stresses are negligible in both the inner and outer regions if

$$\beta\,\sigma T_o/(\rho_\ell Q H_s T_c) \ll 1, \quad \Delta T/(T_c\Theta^2) \ll 1. \tag{A 1a,b}$$

(A 1a) ensures that the thermocapillary stress in the inner region is negligible compared with the viscous stress due to the evaporatively induced flow, while (A 1b) ensures that the pressure field due to the outer thermocapillary flow does not perturb the interface. We show that these conditions hold in Kim's experiments; the modest discrepancy between theory and experiment is not due to thermocapillarity.

We derive (A 1a) first. Within the inner region, the dimensional film thickness $H_* \sim H_s$. In the lubrication approximation, the shear stress within the film owing to the evaporatively induced flow $\mu_\ell U_{*y} \sim H_* P_{*x}$. Because the thermocapillary stress $\sim \sigma'(T_*)T_{*x}$, the ratio of thermocapillary to viscous stress $\sim \sigma'(T_*)T_{*x}/H_*P_{*x}$. We now estimate T_{*x}, P_{*x} and $\sigma'(T_*)$. First, to find T_{*x}, we eliminate J between (6a) and (6b) to show that $1-T = \beta H(1+P)/(1+\beta H)$. Within the inner region, $H\sim 1$ and $-1 < P < 0$, so the dimensionless temperature difference $\sim\beta$. So $T_x\sim\beta$ and the dimensional temperature gradient $T_{*x}\sim\beta\Delta T/L_s$. Secondly, $P_{*x}\sim P_s/L_s$, since the pressure difference driving the inner flow $\sim P_s$, i.e. $\rho_\ell Q\Delta T/T_o$ by (4a). That pressure difference occurs on the inner scale L_s by the analysis in § 5. Thirdly, $\sigma'(T)\sim\sigma/T_c$, where T_c is the critical temperature (see e.g. Morris 2000, p. 66) The ratio of thermocapillary to viscous stress is therefore $\beta\,\sigma T_o/(\rho_\ell Q H_s T_c)$, so that thermocapillarity is negligible within the inner region if (A 1a) holds. Usually, $\rho_\ell > 500\,\mathrm{kg\,m^{-3}}$, $Q > 0.5\,\mathrm{MJ\,kg^{-1}\,K^{-1}}$, $H_s > 1\,\mathrm{nm}$ and $\sigma < 20\,\mathrm{mN\,m^{-1}}$; in particular, these conditions hold in Kim's experiments. So $\sigma/(\rho_\ell Q H_s) < 0.1$, and (A 1$a$) is satisfied as $T_o < T_c$ and $\beta \ll 1$. Thermocapillarity is thus negligible within the inner region since high shear stresses are induced in the thin film by the evaporatively imposed flow.

Next we derive (A 1b), and show that thermocapillarity is also negligible in the outer region. Morris (2000, p. 66) uses scaling to show that the normal velocity $V_{\ell M}$ due to thermocapillarity is related to the evaporatively induced normal velocity

V_ℓ by $V_{\ell M}/V_\ell \sim \Theta^2 \Delta T/(Ca\, T_c)$, where $Ca = \mu_\ell V_\ell/\sigma$, as throughout this work. The thermocapillary flow induces a pressure field that can be estimated from the lubrication equation. By repeating the analysis in Morris (2000, p. 65), we find that this pressure difference causes a change $\Delta\Theta$ across the outer region given by $\Delta\Theta/\Theta \sim \mu_\ell V_{\ell M}/(\sigma\Theta^4)$. By combining this result with that for $V_{\ell M}/V_\ell$, we find that $\Delta\Theta/\Theta \sim \Delta T/(T_c\Theta^2)$. So, thermocapillarity is negligible within the outer region if $\Delta T/(T_c\Theta^2) \ll 1$, as stated by (A 1*b*). This analysis strengthens slightly the conclusions reached by Morris (2000, p. 66); there we state that $V_{\ell M}/V_\ell < 1$, but do not state explicitly that thermocapillarity is therefore negligible since pressure differences due to V_ℓ are themselves too small to perturb the interface. Thermocapillarity is negligible in the outer region in Kim's experiments since $\Delta T < 0.5\,\mathrm{mK}$, $T_c > 500\,\mathrm{K}$ and $\Theta > 0.01$ so that $\Delta T/(T_c\Theta^2) < 0.01$.

Appendix B. Derivation of the one-parameter family of solutions (14)

By (11), $y = \hat{H}/(x\sqrt{2})$ satisfies

$$4y^3(y_{zzz} - y_z) = -1 \quad \text{where} \quad z = \ln(x/k) \tag{B 1}$$

as in (14). We show that the assumption $y_z \gg y_{zzz}$ for $z \to \infty$ leads to a self-consistent solution of the differential equations (13*a*, *b*) that satisfies the outer boundary condition (13*f*), namely $\hat{H}_{xx}(\infty) = 0$.

If $y_z \gg y_{zzz}$ for $z \to \infty$, (B 1) implies $4y^3 y_z = 1 + o(1)$ for $z \to \infty$. By integration, $y \sim z^{1/4}$ where we have absorbed the integration constant into the parameter k. Since $y \sim z^{1/4}$ satisfies the condition $y_z \gg y_{zzz}$, the assumption is self-consistent, and $\hat{H} \sim xz^{1/4}\sqrt{2}$. This gives the first term in (14). Higher-order terms can be found by writing (B 1) as $4y^3 y_z = 1 + 4y^3 y_{zzz}$, and using successive approximations. All integration constants arising in successive integrations must be taken as zero; since the condition $y_z \gg y_{zzz}$ reduces the order of the differential equation to one, the solution can depend on only the one parameter k. To systematize those calculations, we let $w = y/z^{1/4}$ so that w satisfies

$$w = \{3w_{zz} + 4zw_{zzz} - (4z + \tfrac{9}{4}z^{-1})w_z + w^{-3}\}/\{1 - \tfrac{21}{16}z^{-2}\}, \tag{B 2}$$

without approximation. As (B2) is invariant under $z \to -z$, it admits a solution $w \sim \sum_{n=0}^{\infty} A_n/z^{2n}$, and (14) follows by substitution. Though this expansion for w involves only even powers of $z = \ln(x/k)$, w is not an even function of $\ln(x/k)$ for all x because the expansion includes only terms that are merely logarithmically small as $x \to \infty$; algebraically small terms are not included.

REFERENCES

Anderson, D. M. & Davis, S. H. 1995 The spreading of volatile liquids on heated surfaces. *Phys. Fluids* **7**, 248–265.

Cammenga, H. K. 1980 Evaporation mechanisms of liquids. In *Current topics in materials science* (ed. E. Kaldis), chap. 4. North-Holland.

Cox, R. G. 1986 The dynamics of spreading of liquids on a solid surface. Part 1. Viscous flow. *J. Fluid Mech.* **168**, 169–194.

DasGupta, S., Schonberg, J. A., Kim, I. Y. & Wayner, P. C. 1993 Use of the augmented Young–Laplace equation to model equilibrium and evaporating extended menisci. *J. Colloid Interface Sci.* **157**, 332–342.

Delhaye, J. M. 1974 Jump conditions and entropy sources in two–phase systems, *Intl J. Multiphase Flow* **1**, 395–409.

Fisher, L. R. & Israelachvili, J. N. 1981 Experimental studies on the applicability of the Kelvin equation to highly curved concave menisci. *J. Colloid Interface Sci.* **80**, 528–541.

Hocking, L. M. 1995 On contact angles in evaporating liquids. *Phys. Fluids* **7**, 2950–2955.

Joanny, J. F. 1986 Dynamics of wetting: interface profile of a spreading liquid. *J. Mec. Theor. Appl.* Special issue, pp. 249–271.

Kim, I. Y. 1994 An optical study of the heat transfer characteristics of an evaporating thin liquid film. PhD thesis, Rensselaer Polytechnic Institute, Troy, New York.

Kim, I. Y. & Wayner, P. C. 1996 Shape of an evaporating completely wetting extended meniscus. *J. Thermophys. Heat Transfer* **10**, 320–325.

Levinson, P., Valignat, M. P., Fraysse, N., Cazabat, A. M. & Heslot, F. 1993 An ellipsometric study of adsorption isotherms. *Thin Solid Films* **234**, 482–485.

Miller, C. A. & Ruckenstein, E. 1974 The origin of flow during wetting of solids. *J. Colloid Interface Sci.* **48**, 368–373.

Moosman, S. & Homsy, G. M. 1980 Evaporating menisci of wetting fluids. *J. Colloid Interface Sci.* **73**, 212–223.

Morris, S. J. S. 2000 A phenomenological model for the contact region of an evaporating meniscus on a superheated slab. *J. Fluid Mech.* **411**, 59–89.

Muller-Buschbaum, P., Tolan, M. & Press, W. 1994 X–ray study of the wetting behaviour of CCl_4 on Si/SiO_2 surfaces. *Z. Phys.* B **95**, 331–339.

Potash, M. & Wayner, P. C. 1972 Evaporation from a two dimensional extended meniscus. *Intl J. Heat Mass Transfer* **15**, 1851–1863.

Reyes, R. & Wayner, P. C. 1996 A Kelvin–Clapeyron adsorption model for spreading on a heated plate. *Trans. ASMEC: J. Heat Transfer* **118**, 822–829.

Schonberg, J. A., Dasgupta, S. & Wayner, P. C. 1995 An augmented Young–Laplace model of an evaporating meniscus in a microchannel with high heat flux. *Exp. Therm. Fluid Sci.* **10**, 163–170.

Stephan, P. C. 1992 Wärmedurchgang bei Verdampfung aus Kapillarrillen in Wärmerohren. *Fortschr.–Ber. VDI Reihe* 19, No. 59. VDI, Dusseldorf.

Stephan, P. C. & Busse, C. A. 1992 Analysis of the heat transfer coefficient of grooved heat pipe evaporator walls. *Intl J. Heat Mass Transfer* **35**, 383–391.

Tanner, L. H. 1979 Spreading of silicone oil drops on horizontal surfaces. *J. Phys.* D **12**, 1473–1484.

Thompson, P. A. & Troian, S. M. 1997 A general boundary condition for liquid flow at solid surfaces. *Nature* **389**, 360–362.

Truong, J. G. & Wayner, P. C. 1987 Effects of capillary and van der Waals dispersion forces on the equilibrium profile of a wetting liquid – theory and experiment. *J. Chem. Phys.* **87**, 4180–4188.

Wong, H., Morris, S. & Radke, C. J. 1992 Three dimensional menisci in polygonal capillaries. *J. Colloid Interface Sci.* **148**, 317–336.